InSAR-based characterization of rock glacier movement in the Uinta Mountains, Utah, USA

George Brencher[1], Alexander L. Handwerger[2,3], Jeffrey S. Munroe[1]

[1]Geology Department, Middlebury College, Middlebury, 05753, USA
5 [2]Joint Institute for Regional Earth System Science and Engineering, University of California, Los Angeles, 90095, USA
[3]Jet Propulsion Laboratory, California Institute of Technology, Pasadena, 91109, USA

Correspondence to: George Brencher (qbrencher@gmail.com)

Abstract. Rock glaciers are a prominent component of many alpine landscapes and constitute a significant water resource in some arid mountain environments. Here, we employ satellite-based interferometric synthetic aperture radar (InSAR) between 10 2016 and 2019 to identify and monitor active and transitional rock glaciers in the Uinta Mountains (Utah, USA), an area of ~3,000 km^2. We used mean velocity maps to generate an inventory for the Uinta Mountains containing 205 active and transitional rock glaciers. These rock glaciers are 11.9 ha in area on average and located at a mean elevation of 3308 m, where mean annual air temperature is -0.25 ˚C. The mean downslope velocity for the inventory is 1.94 cm/yr, but individual rock glaciers have LOS velocities ranging from 0.35 to 6.04 cm/yr. To search for relationships with climatic drivers, we investigated 15 the time-dependent motion of three rock glaciers. We found that rock glacier motion has a significant seasonal component, with rates that are more than 5 times faster during the late summer compared to the rest of the year. Rock glacier velocities also appear to be correlated with the snow-water equivalent of the previous winter's snowpack. Our results demonstrate the ability to use satellite InSAR to monitor rock glaciers over large areas and provide insight into the environmental factors that control their kinematics.

1 Introduction

Rock glaciers are bodies of ice and rock debris that creep downslope due to deformation of their internal ice-rock mixture (Fig. 1) (Wahrhaftig and Cox, 1959; Barsch, 1996). They play an important role in alpine hydrology and landscape evolution, principally through the release of seasonal meltwater and the continuous downslope transport of coarse material (Azócar and Brenning, 2010; Frauenfelder and Kääb, 2000). They also constitute a significant water resource in arid regions (Schaffer et 25 al., 2019), and their importance as a water source is likely to increase with ongoing climate change (Jones et al., 2018a). Understanding how rock glaciers respond to changes in climate is therefore a necessary part of predicting the evolution of cold mountain environments.

Active rock glaciers contain internal ice, exhibit coherent downslope movement over most of their surface, and move 30 downslope at rates on the order of a decimeter to several meters per year (IPA Action Group Rock Glacier Inventories and

Kinematics, 2020). Rock glaciers moving at slower rates (<10 cm/yr) are defined as transitional and can evolve towards an active or inactive state depending on their topographic and climatic setting (IPA Action Group Rock Glacier Inventories and Kinematics, 2020). Controls on rock glacier kinematics are numerous, and include time-dependent water and talus delivery, internal rock glacier structure, bedrock geometry, and short and long-term changes in ground temperature (Haeberli et al.,

35   2006; Kääb et al., 2007; Ikeda et al., 2008; Delaloye et al., 2010; Müller et al., 2016; Kenner et al., 2017). As with ice glaciers (e.g. Bartholomew et al., 2010; Iverson, 2010; Minchew and Meyer, 2020), tectonic faults (e.g. Bürgmann, 2018) and landslides (e.g. Bayer et al., 2018; Handwerger et al., 2019), liquid water and pore-water pressure are also important drivers of short-term rock glacier motion (Ikeda et al., 2008; Moore, 2014; Kenner et al., 2017; Eriksen et al., 2016; Cicoira, 2019; Fey and Krainer, 2020).

40

Rock glacier velocity has been shown to vary over temporal scales ranging from multi-year to hourly (Delaloye et al., 2010; Kenner et al., 2017). For instance, rock glaciers in the European Alps and Norway have undergone significant long-term acceleration in the past few decades attributed to warming permafrost temperatures (Delaloye et al., 2010; Kääb et al., 2007; Kaufmann and Ladstädter, 2007; Roer et al., 2005; Vonder Muehll et al., 2007; Ikeda et al., 2008; Kenner et al., 2017; Eriksen

45   et al., 2018; Fey and Krainer, 2020). On a multi-year time scale, temperature is thought to primarily control variations in rock glacier velocity (Arenson et al., 2002; Haeberli et al., 2006), although differences in precipitation between years may also explain contrasts in rock glacier movement (Ikeda et al., 2008). Seasonal variations in rock glacier motion are also well documented (Haeberli, 1985; Kääb et al., 1997; Arenson et al., 2002) and typically manifest as a strong acceleration in the late spring coincident with melting of snow and ice, followed by a gradual deceleration in the late fall and winter (Perruchoud and

50   Delaloye, 2007; Liu et al., 2013). Recent work suggests that spring acceleration is driven by melt water infiltration that increases pore-water pressure and reduces frictional strength along shear horizons within rock glaciers (Kenner et al., 2017; Cocoira et al., 2019; Fey and Krainer, 2020). Heavy precipitation and snowmelt events have also been observed to coincide with short-term rock glacier acceleration (Wirz et al., 2016; Kenner et al., 2017).

55   Access to high-resolution remote sensing imagery and digital topography has improved our ability to inventory rock glaciers over large areas (Krainer and Ribis, 2012; Rangecroft et al., 2014; Falaschi et al., 2014; Roudnitska et al., 2016; Jones et al., 2018b; Brardinoni et al., 2019). Such datasets are important for assessing the past and current distributions of mountain permafrost, understanding landscape response to climate change following the last glacial maximum, and appraising the regional water storage potential of rock glaciers (Lieb, 1996; Boeckli et al., 2012; Schmid et al., 2015; Zasadni and Kłapyta,

60   2016; Azócar and Brenning, 2010; Jones et al., 2018a). However, most remote-sensing based inventories have used optical images to identify rock glaciers based on morphology alone and are therefore incapable of determining whether features are currently moving and thus likely contain ice (Munroe, 2018; Nicholson et al., 2009; Lilleøren and Etzelmüller, 2011; Kellerer-Pirklbauer et al., 2012; Rangecroft et al., 2014; Roudnitska et al., 2016). Optical imagery is also limited to daytime acquisitions,

and snow, shadow, and clouds can obscure features on the ground, sometimes leading to undercounting of rock glaciers

65 (Villarroel et al., 2018).

An alternative approach to inventory rock glaciers is interferometric synthetic aperture radar (InSAR), a remote sensing technique that is not affected by cloud cover, can operate day or night, can sometimes reveal deformation even in the presence of snow, and can detect motion on the millimeter scale (e.g., Liu et al., 2013; Villarroel et al., 2018; Kääb et al., 2021; Strozzi

70 et al., 2020). InSAR does have limitations germane to the study of rock glaciers, including underestimation of true 3D velocities, complications arising from the fixed one-dimensional look direction of the satellite, atmospheric delay, poor correlation caused by changes in ground cover such as snow to snow-free conditions, and errors associated with features moving at velocities greater than the deformation threshold related to the radar wavelength. Many of these can be mitigated by careful study design, however, and at the scale of range-wide analysis, significant patterns in rock glacier kinematics can

75 still be identified.

InSAR has been effectively used to create rock glacier inventories of varying extents and to study rock glacier kinematics (e.g. Nagler et al., 2002; Rignot et al., 2002; Kenyi and Kaufman, 2003; Strozzi et al., 2004; 2020; Lilleøren et al., 2013; Lui et al., 2013; Barboux et al., 2014; Rick et al., 2015; Necsoiu et al., 2016; Wang et al., 2017; Villarroel et al., 2018). Previous InSAR-

80 aided studies of rock glaciers generally fall into two groups: 1) studies that leverage InSAR to facilitate inventorying of large numbers of rock glaciers (e.g. Villarroel et al. (2018) mapped 2,116 rock glaciers) over large regions (e.g. Wang et al. (2017) examined an area of 63,000 km^2) or 2) studies that apply InSAR for in-depth kinematic analysis of one or a few rock glaciers (e.g. Rignot et al. 2002; Kenyi and Kaufman, 2003; Necsoiu et al., 2016). We combine these two approaches by inventorying rock glaciers over an area of roughly 3,000 km^2, estimating velocity for all rock glaciers in our inventory, and performing

85 displacement time series analysis on three representative rock glaciers. Our interpretations of our inventory results and kinematic results inform one another, forming a more comprehensive picture of Uinta rock glacier characteristics and dynamics.

Given the importance of rock glaciers as features of high mountain landscapes, their contribution to mountain hydrology, their

90 ability to act as permafrost indicators, and the remaining open questions about climatic controls on their behavior, additional work is needed to develop the robust understanding of rock glacier dynamics necessary for predicting the response of these features to future climate change (Eriksen et al., 2018). Here, we investigate rock glaciers in the Uinta Mountains (Utah, USA), an important headwater region for the Colorado River in the southwestern USA. Nearly 400 rock glaciers have been visually identified in these mountains, but the presence of ice has been indirectly investigated in only two, limiting

95 understanding of slope processes, hydrology, and permafrost extent in this region (Munroe, 2018). The method of rock glacier identification employed in a previous study by Munroe (2018) involved examining the bases of high-angle bedrock and talus slopes for steep-fronted bulges with reduced lichen cover and ridges and furrows characteristic of rock glaciers using visual

imagery at a 1:5,000 scale. In contrast, we use satellite-based InSAR alongside visual imagery to identify active and transitional rock glaciers and to evaluate controls on their rates of motion over seasonal to multi-annual time scales (2016-2019). Our work

100   is the first to use satellite InSAR to investigate rock glacier motion in the Uinta mountain range.

2 Study area

The Uinta Mountains are an east-west trending mountain range extending over ~3,000 km^2 in northeastern Utah, USA (Fig. 2). The bedrock of the Uinta Mountains (hereafter, the "Uintas") is Precambrian quartzite, sandstone, and argillite uplifted during the Laramide Orogeny (70–80 Ma) (Bradley, 1936; Sears et al., 1982; Dehler, 2007). While the Uintas are not currently

105   glacierized, during the late Pleistocene, valley glaciers covered more than 2,000 km^2, creating well-developed glacial geomorphology (Munroe and Laabs, 2009).

Climate at higher elevations in the Uintas (> 3,000 m) is periglacial, with a mean annual air temperature (MAAT) from 1981–2010 ranging from -4.0 to 3.3 ℃ (Fig. 2b). Future climate conditions have not been modelled specifically for the Uintas, but

110   Atmosphere–Ocean General Circulation Models for the western U.S. parameterized with the A1B "business as usual" emissions scenario predict an increase in air temperature of about 1.5° C by 2030 (IPCC, 2018). Mean annual precipitation (MAP) in the Uintas between 1981 and 2010 ranged from 45 to 107 cm (Fig. 2c). Most precipitation falls in the winter as snow, of which the largest quantities fall in the western part of the range. The Uintas are an important water resource in the state of Utah, supplying water to 17 counties for municipal, industrial, and agricultural purposes (Tingstad, 2010). Furthermore,

115   calculations indicate that 10–15% of the Colorado River flow at Lees Ferry, Arizona, is comprised of water from northeastern Utah (Tingstad, 2010). Flow of the Colorado River is expected to decline 10–30% from 2008 levels in the next 18 to 38 years based on streamflow modelling work, implying intense water deficits in the Colorado River system over the next century (Barnett and Pierce, 2008).

120   Rock glaciers and talus in the Uintas are estimated to store 0.14 km^3 of water, or ~10–35% of the range's annual runoff (Munroe, 2018). These rock glaciers could constitute an even more significant water resource in the coming years as climate change alters temperature and precipitation regimes in the western U.S., particularly during the late summer and autumn when there is less precipitation (MacDonald and Tingstad, 2007). Previous work identified 395 rock glaciers in the Uintas (Munroe, 2018). One of the primary goals of our study was to update this existing inventory, which was based solely on rock glacier

125   morphology, and to identify which of these features are active, transitional, and inactive using the definitions from the IPA Action Group Rock Glacier Inventories and Kinematics (2020).

3 Methods

3.1 InSAR analysis

Copernicus Sentinel-1 radar data covering the Uinta Mountains were downloaded from the Alaska Satellite Foundation Vertex
130 website (https://vertex.daac.asf.alaska.edu/). We used data acquired in the interferometric wide swath (IW) mode, collected
between August 2016–October 2019. We further selected SAR images acquired when the Uinta rock glaciers appeared to be
largely snow-free in optical Planetlab imagery (https://www.planet.com/explorer/). We downloaded 26 SAR scenes on
ascending track 122 (satellite moving north looking east) and 32 SAR scenes on descending track 27 (satellite moving south
looking west). During the snow-free period in 2018, only one ascending and descending track SAR scene was available. Each
135 SAR scene has a pixel size of 14.1 m in azimuth (i.e., along-track direction) and 2.3 m in range (i.e., look direction).

Interferograms were processed in the JPL InSAR Scientific Computing Environment (ISCE) version 2 software (Rosen et al.,
2012) with two looks in range and one look in azimuth, resulting in a ~5 m by ~14 m pixel size. Within a given summer (i.e.,
snow-free period), all possible combinations of interferograms were processed (Fig A1; Table A1). Late summer scenes were
140 combined with scenes from the following summers to create year-long pairs that bridge the winter when the ground is covered
in snow. In total we created 45 ascending pairs and 63 descending pairs for a total of 108 interferograms. The minimum time
between pairs was 6 days and the maximum time was 756, with a median of 48 days. We used a Shuttle Radar Topography
Mission (SRTM) DEM with ~30 m pixel spacing to remove topographic signal from the phase and to geocode the
interferograms. In addition, selected one-year interferogram pairs were reprocessed with a USGS 3DEP DEM with 10 m pixel
145 spacing. The primary reason we reprocessed these selected pairs was to improve spatial resolution in order to more accurately
inventory the moving rock glaciers (Table A1). However, computational limitations prevented us from processing all 108
interferograms with the 10 m DEM. Interferograms were unwrapped using the Statistical-Cost, Network-Flow Algorithm for
Phase Unwrapping (SNAPHU) (Chen and Zebker, 2002). We applied a correlation threshold of 0.3 during unwrapping to
remove low-quality data.

150

Many of the interferograms suffered from topography-correlated atmospheric effects that obscured signals of rock glacier
deformation. These atmospheric effects result from differences in pressure, temperature, and relative humidity in the lower
troposphere, causing radar to refract variably over the land surface, and producing a 2-way phase delay (Bekaert et al., 2015).
We applied a tropospheric phase delay correction based on pressure, temperature, and humidity predictions from the ERA-I
155 global weather model, which outputs data at a spatial resolution of 80 km on a 6 hour interval (Bekaert et al., 2015). The
correction was done using the TRAIN software package (Toolbox for Reducing Atmospheric InSAR Noise) from Bekaert et
al. (2015).

All resulting InSAR velocity maps were used along with Google Earth imagery, the USGS 10 m DEM, and the previous Uinta

160   rock glacier inventory (Munroe, 2018) to generate a new rock glacier inventory in QGIS 3.10. We inventoried rock glaciers displaying a clear and relatively high LOS velocity signal with a sign suggesting downslope movement (Fig. 2). The smallest spatial area we considered to have a clear and coherent signal indicating rock glacier activity was 5,000 m². Rock glaciers identified in the Munroe (2018) inventory that showed no coherent and distinct deformation in our InSAR velocity maps were classified as inactive. Boundaries of rock glaciers were manually delineated on the basis of morphology and InSAR-derived

165   movement pattern. Slope, aspect, and elevation of features in the rock glacier inventory were calculated in QGIS from the 10 m DEM. Rock glaciers were classified as lobate (width > length) or tongue-shaped (length > width) (Barsch, 1996) based on morphology. We also grouped the rock glaciers into "North Uintas" or "South Uintas" based on their location relative to the east-west trending spine of the mountain range (Fig. 2). A non-parametric Kruskall-Wallis test with a significance threshold of 0.05 was used to establish significance of differences between all rock glacier groups.

170

Average annual velocities for rock glaciers were calculated in QGIS using velocity maps derived from ascending and descending stacks of one-year interferograms (Fig. 2). These stacks were calculated from the one-year pairs with 10 m pixel spacing (Table A1). Average LOS velocity magnitudes were calculated by taking the mean of the absolute value of velocity values over the surface of each rock glacier. We then defined characteristic LOS rock glacier velocities as the 75th percentile

175   of the absolute value of velocity values within a mapped rock glacier body. This approach was used to deemphasize noisy areas that could contain erroneous high or low velocities and to highlight the velocity of the active part of each rock glacier (Bayer et al., 2018; Handwerger et al. 2019). For both mean and 75th percentile velocity, two values were generated for each rock glacier, one derived from the ascending and another from the descending stack.

180   To quantify uncertainty, InSAR-derived LOS velocities for 12 mostly flat, roughly rock-glacier sized control areas were calculated using the absolute value of the same ascending and descending stacks used to calculate rock glacier velocity. We assumed these control areas are stable (i.e., not deforming) and therefore any apparent deformation is due to uncertainty.

In addition to our LOS velocity estimates, we calculated ground surface velocity estimates for each rock glacier by projecting

185   our LOS estimates onto the downslope direction using the method described in Liu et al. (2013). This approach assumes that rock glaciers are flowing uniformly along their average azimuth and slope direction. The heading angle and incidence angle of the satellite are ~12˚ (positive counter clockwise from North) and ~41˚ for the ascending track and ~168˚ and ~40˚ for the descending track. The USGS 10 m DEM was used to calculate average slope angle and average azimuth angle for each rock glacier and the 75th percentile LOS velocities were used to represent LOS velocity. The larger of the resulting ascending and

190   descending values is used to represent rock glacier velocity in our analysis.

Lastly, we performed time series inversions for three representative rock glaciers selected on the basis of their clear deformation signal in the average velocity stack: Grayling Lake, Whiterocks River, and Rockflour Lake (Fig. 3). Time series were calculated for these rock glaciers using the Small Baseline Subset (SBAS) method (Berardino et al., 2002; Schmidt and

195   Bürgmann, 2003). Interferograms with low overall coherence were manually removed from the time series. Stable local reference points for each rock glacier were chosen using Google Earth imagery to identify nearby ridge tops (Fig. 3).

3.2 Climate Data

Climatic data relevant to the rock glacier inventory were obtained by two sources: Parameter-elevation Regressions on Independent Slopes Model (PRISM, PRISM Climate Group, Oregon State University, http://prism.oregonstate.edu) and Snow

200   Telemetry (SNOTEL, https://www.wcc.nrcs.usda.gov/snow/). PRISM data were used to establish the temperature and precipitation envelope of the rock glacier inventory. We downloaded 30 year normal (1981–2010) mean temperature and precipitation rasters with 800 m pixel spacing for each month with the PRISM package in R and used them to calculate mean annual air temperature (MAAT) and precipitation (MAP) for each rock glacier in the inventory. SNOTEL data (1980–2020) were used to constrain meteorological conditions during the intervals represented by the cumulative displacement time series.

205   The Chepeta SNOTEL, at an elevation of 3200 m, is 10.0 km from the Whiterocks River rock glacier (3460 m) and 8.1 km from the Rockflour Lake rock glacier (3301 m) (Fig. 2). The Five Points Lake SNOTEL, at an elevation of 3335 m, is 11.8 km from the Grayling Lake rock glacier (3101 m).

4 Results

4.1 Rock glacier inventory

210   Our inventory contains 205 rock glaciers totalling 24.3 km^2 that are found at an average elevation of 3307 ± 169 m (± corresponds to 1 standard deviation) (Fig. 4d). The rock glaciers average 11.9 ± 11.0 ha in area; 7% are >30 ha, with a maximum of 60.2 ha (Fig. 4a). Their average slope is 22.1˚ ± 4.6˚ (Fig. 4g). The rock glaciers most frequently face north (20.5%), followed by northeast (17.5%), and east (12.2%) (Fig. 5a, b). For reference, steep slopes of the Uintas (>10˚) face generally north (18.7%) and south (19.6%) (Fig. 5c).

215

Morphologically, 78.5% of the rock glaciers are lobate and 21.5% are tongue-shaped. Tongue-shaped rock glaciers are found at average elevations of 3384 ± 192 m, significantly higher than lobate rock glaciers, which are found at average elevations of 3286 ± 156 m (n = 205, p = 0.000) (Fig. 4e). Lobate rock glaciers average 13.1 ha ± 11.9 ha in area, significantly larger than tongue-shaped rock glaciers, which are 7.40 ± 4.15 ha on average (n = 205, p = 0.017) (Fig. 4b). All rock glaciers >20 ha in

220   area are lobate rock glaciers and morphology is not correlated with rock glacier slope or aspect.

A total of 44 rock glaciers (21.5% of the inventory) are located on the north side of the Uintas. These features are found at average elevation of 3361 ± 102 m, significantly higher than the 161 rock glaciers located on the south side, which are found at 3292 ± 180 m (n = 205, p = 0.0177) (Fig. 4f). Rock glaciers on the north side tend to face broadly northeast, with 43.2% facing north and 25.0% facing northeast, while rock glaciers on the south side do not appear to prefer a specific aspect as strongly. Area and slope angle are not significantly different for North and South Uintas rock glaciers (Fig. 4c, i). Tongue-shaped rock glaciers make up a larger proportion of North Uintas rock glaciers (31.8%) than the South Uintas rock glaciers (18.6%).

4.2 Rock glacier temperature and precipitation

Given the PRISM dataset, rock glaciers are found at an average MAAT of -0.25 ± 1.08 ˚C (Fig. 4j). 90.7% of the rock glaciers are found at MAATs above -1.5 ˚C. Average MAAT at lobate rock glaciers is -0.13 ± 1.0 ˚C, significantly higher than tongue-shaped rock glaciers, which are found at an average MAAT of -0.66 ± 1.2 ˚C (n = 205, p = 0.000) (Fig. 4k).

Rock glaciers receive an estimated average of 75.0 ± 8.47 cm of precipitation per year, (Fig. 4m) of which ~29–40% is rain and ~60–71% is snow. North Uinta rock glaciers receive on average 81.6 ± 7.85 cm, significantly more than South Uinta rock glaciers, which receive 73.2 ± 7.72 cm (n = 205, p = 0.000) (Fig. 4o). Tongue-shaped rock glaciers receive 77.8 ± 10.4 cm, significantly more than the 74.2 ± 7.73 cm received by lobate rock glaciers (n = 205, p = 0.031).

4.3 Inactive rock glaciers

Of the rock glaciers identified during this study and previously by Munroe (2018), 199 are inactive based on our InSAR velocity maps. These inactive rock glaciers, which total 12.9 km^2, average 6.5 ± 6.3 ha in area, and are found at an average elevation of 3,269 ± 142 m (Fig. 6a, b). Their average MAAT is 0.035 ± 0.91 ˚C, and average MAP is 78.3 ± 8.82 cm (Fig. 6c, d). They are significantly smaller than the active and transitional rock glaciers and receive significantly more precipitation (area, n = 404, p = 0.000; precipitation, n = 404, p = 0.000) (Fig. 6a, d). They also experience significantly higher MAATs (n = 404, p = 0.001) (Fig. 6c) and are found at significantly lower elevations (n = 404, p = 0.002). They face north most commonly, at 22.6% of the time, followed by south, 17.1 percent of the time. They face north more slightly more often than active and transitional rock glaciers, which face north 20.5% of the time.

4.4 Rock glacier velocity

Uinta rock glaciers generally have non-uniform spatial velocity patterns. On their rooting zone, rock glacier velocity tends to be highly heterogenous, varying over ~10 m length scales. On the main body of the rock glaciers, velocity is typically more homogenous, with one or more high velocity patches surrounded by areas of a lower velocity. For many rock glaciers, these high-velocity patches occupied only a small portion of the total surface area of the rock glacier. In projecting rock glacier velocities downslope, 75th percentile LOS velocities were scaled by a factor between 1.06 and 6.10. The characteristic

downslope velocity from 2016–2019 was 1.94 ± 1.16 cm/yr (Fig. 7b). The fastest rock glacier velocities occurred during August each year, when several rock glaciers had maxima above 40 cm/yr. No metric of rock glacier velocity is significantly correlated with rock glacier area, elevation, slope, or type (i.e. lobate or tongue-shaped) (Fig. 7a, Fig. A2). North and south facing rock glaciers had higher downslope velocities than broadly east and west facing rock glaciers (Fig A2f).

We approximated uncertainty in the InSAR velocity by quantifying the apparent velocity of 12 stable control areas. We found that average LOS velocities for stable areas was 0.33 ± 0.12 cm/yr and 0.62 ± 0.32 cm/yr for ascending and descending stacks respectively.

Time series for the three representative rock glaciers show time-dependent deformation from 2016–2019 (Fig. 8a, b, c). Each of these rock glaciers had faster LOS velocities during snow-free observation periods than during snow-covered periods (n =30, p = 0.001) (Fig. 8d). For example, the Grayling Lake rock glacier averaged 4.97 cm/yr during snow-free observation periods and 0.83 cm/yr during snow-covered periods.

In addition to seasonal changes in velocity, the Rockflour Lake rock glacier experienced a strong deceleration throughout 2018 (Fig. 8c). This rock glacier appears to have ceased motion the winter of 2017/18 and only displaced 0.11 cm during the subsequent summer, fall, and winter of 2018. Yet during the same time period in 2016 and 2017, this rock glacier displaced 4.0 cm and 1.79 cm, respectively. This change in behavior corresponds temporally with a reduced spring melt caused by a small winter snowpack (Fig. 9).

5 Discussion

5.1 The rock glacier niche

The rock glacier inventory we created reveals the locations of active and transitional rock glaciers in the Uintas and illuminates the conditions necessary for rock glacier formation and sustained creep. Although the Uintas extend from elevations of ~2200 m to > 4100 m, 77.1% of rock glaciers are found in a narrow elevation band between 3100 and 3500 m. This zone has a MAAT from 0.5 to -2 °C, where talus production is likely high due to frost-cracking (Hales and Roering, 2007; Rempel et al., 2016). Deposition of fresh talus onto the rock glacier source area helps sustain rock glacier motion (Barsch, 1996; Müller et al., 2016). The comparison between our active and transitional rock glacier inventory and the inactive rock glaciers identified by the previous inventory (Munroe, 2018) demonstrates the sensitivity of Uinta rock glaciers to temperature. Active and transitional rock glaciers are found at higher elevations than inactive rock glaciers and have a subzero median MAAT, whereas inactive rock glaciers have a median MAAT above zero (Fig. 6c). Rock glaciers can become inactive for myriad reasons, but almost all are related to insufficient internal ice or insufficient talus supply (Barsch, 1996). Both talus production and stability of internal ice are related to temperature, as freeze-thaw cycles strongly control erosion and temperature is the primary control

285 on permafrost stability (Hales and Roering, 2007; Hinzman, 1998). Depending to some extent on local conditions, permafrost begins to degrade at MAATs above 0 °C (Hoelzle and Haeberli, 1995), reducing ice content and rendering rock glaciers inactive.

Tongue-shaped rock glaciers are found at significantly higher elevations than lobate rock glaciers. Noting a similar trend in
290 the Colorado Front Range, Janke (2007) concluded that high-elevation tongue-shaped rock glaciers evolve from ice glaciers that become covered by debris. We cannot evaluate this theory with our data; however, in the Uintas, well-developed cirques are found mostly at high elevations (>3250 m), while steep valley walls continue down below the elevation where active rock glaciers are observed (Munroe and Laabs, 2009). Tongue-shaped rock glaciers are mostly found in these high-elevation cirques, which, as a function of their geometry, may simply be more likely to produce tongue-shaped rock glaciers if debris is
295 supplied from a narrow zone at the base of the cirque headwall (Degenhardt, 2009). In contrast, lobate rock glaciers are mostly found along valley walls, where debris is produced more consistently across a wider area (Degenhardt, 2009).

The geometry of the Uintas can explain other trends in rock glacier location. For instance, active and transitional rock glaciers in the North Uintas preferentially face northeast, while active and transitional rock glaciers in the South Uintas appear to have
300 no strong preference for aspect. This north-facing trend in North Uintas rock glaciers is likely related to slope patterns. The North Uintas are steeper than the South Uintas; as such, high elevation terrain is less extensive, and is found closer to the main east-west trending spine of the range. Thus, most rock glaciers in the North Uintas root on the east-west trending spine, and flow northward, down-gradient. In the South Uintas, active and transitional rock glaciers face all directions in relatively equal proportions. Given that north-facing slopes are less common than south-facing slopes on the south side of the range, South
305 Uintas rock glaciers do face north more often than expected if rock glaciers were distributed randomly over steep mountain slopes. Rock glaciers may preferentially face north due to decreased sunlight exposure on north-facing slopes, which decreases local temperatures (Munroe, 2018). This trend has been reported for other North American rock glaciers (e.g. Luckman and Crockett, 1978; Janke et al., 2007; Johnson et al., 2007; Liu et al., 2013)

310 The interaction between Uinta geometry and temperature further seems to control rock glacier morphology. In the North Uintas, 31.8% of rock glaciers are tongue-shaped, whereas in the South Uintas, 18.6% of rock glaciers are tongue shaped. In the gently sloping South Uintas, even valley walls far from the central spine of the mountains are at low enough temperatures to support rock glaciers, while in the steeper North Uintas, valley wall sites an equal distance from the crest have MAATs well above 0 ˚C, and cannot support rock glaciers (Fig. 2b). These valley walls are associated with more lobate rock glaciers than
315 tongue-shaped rock glaciers. The well-developed cirques associated with tongue-shaped rock glaciers, on the other hand, do not extend far from the spine of the Uintas. Thus, in the South Uintas, lobate rock glaciers are more common than tongue-shaped rock glaciers. In the steeper North Uintas, cirques and valley walls are in more equal proportion in the subzero MAAT zone, explaining the increased relative abundance of tongue-shaped rock glaciers.

5.2 Rock glacier velocity

320   Moving rock glaciers in the Uintas deform downslope at rates between 0.35 and 6.04 cm/yr, with the average feature deforming 1.94 cm/yr. This range of mean velocities is lower than velocities reported for other rock glaciers in the western US and the Alps (Janke et al. 2005, Delaloye et al., 2010). We note, however, that rock glacier velocities are often calculated using different methods. Our velocity measurements correspond to average annual rock glacier velocity; thus, they average over seasonal changes such as the typical winter deceleration. Additionally, in many cases, only a small portion of a large rock glacier is

325   moving. Nonetheless, even after accounting for underestimates produced by our methods, it remains notable that rock glaciers in the Uintas appear to be moving nearly an order of magnitude slower than most other North American rock glaciers (Table 1 in Janke et al., 2005). Almost all moving Uinta rock glaciers would most accurately be described as transitional as opposed to active based on the guidelines from the IPA Action Group Rock Glacier Inventories and Kinematics (2020).

330   Rock glaciers are sensitive to numerous variables that could differ between mountain ranges, possibly influencing rock glacier velocity; these include temperature and precipitation regime (Ikeda, et al., 2008; Eriksen et al., 2018) and talus characteristics and delivery rate (Arenson et al., 2002; Müller et al., 2016). However, despite the broad range of temperature and precipitation conditions throughout the Uintas, there is no apparent relationship between velocity and local MAAT or MAP. Furthermore, if talus characteristics have a strong influence on Uinta rock glacier velocities, we would expect adjacent rock glaciers which

335   receive talus derived from the same bedrock units to have similar velocities. However, slow rock glacier velocities were observed throughout the Uintas, with little local grouping of similar velocities in a manner reflecting bedrock composition (Fig. 7a). Thus, the generally low velocities measured for Uinta rock glaciers are not likely due to consistent differences in climate or talus delivery relative to other mountain ranges. An alternative explanation for low rock glacier velocities in the Uintas is comparatively smaller quantities of internal ice. Most Uinta rock glaciers are found at MAATs close to 0 ˚C, based

340   on 30 year temperature normals from 1980–2010. Thus, many rock glaciers may have experienced a negative mass balance of internal ice as temperatures warmed over the past decade.

  Overall, Uinta rock glacier kinematics are complex and defy simple correlation with rock glacier area, elevation, slope, aspect, or morphology (Fig. A2). These factors likely interact to influence rock glacier rheology alongside additional variables

345   including talus, snow, and meltwater delivery rate, clast size, underlying bedrock geometry, temperature, thickness, pore space, ice content, and shear zone geometry (Haeberli et al., 2006). Complex relationships between kinematics and external and internal factors make it especially challenging to predict rock glacier motion. This reality underscores the benefit of using InSAR (or other remote sensing based kinematic data) to generate rock glacier inventories, allowing for quantifiable observation of rock glacier displacement.

5.3 Limitations of InSAR and Uncertainty Analysis

We encountered some limitations of InSAR that require consideration. The insensitivity of InSAR to movement along the satellite flight direction (i.e., perpendicular to the LOS direction) made it difficult to determine whether some north or south facing rock glaciers were actively deforming. This may have produced a bias in our inventory toward rock glaciers flowing broadly eastward or westward. In the prior Uinta Rock glacier inventory based on morphological data (Munroe, 2018), 22.6% of rock glaciers face north, while 17.1% of rock glaciers faced south. In our active and transitional rock glacier inventory, 20.5% of rock glaciers faced north, and 7.32% of rock glaciers faced south. South-facing rock glaciers may be more likely to become inactive due to increased sunlight exposure, elevated local temperatures, and consequent melting of internal ice and it is reasonable to expect similar proportions of north-facing rock glaciers in both inventories. This was observed, suggesting that bias against north and south-facing rock glaciers is not a significant issue in our inventory. Some rock glacier movement could also have been hidden by InSAR decorrelation or geometry; however, since these issues were quite uncommon in our velocity maps, they are not likely to have produced widespread inaccuracies or systematic bias in our inventory.

The LOS measurements provided by InSAR underestimate the true 3D velocity of rock glaciers. For rock glaciers with a larger relative component of northward or southward motion, this underestimate is more extreme. In our inventory, North Uintas rock glaciers, which preferentially face north, have significantly lower LOS velocities than South Uintas rock glaciers, which face more equally in all directions. To better account for this issue, we projected LOS velocities along the downslope direction for each rock glacier. Our approach assumes that rock glacier are flowing uniformly along their average downslope direction. However, for rock glaciers that deform in multiple directions, which is common as they can move vertically upwards and travel along multiple azimuths, our projection could have been inaccurate. In particular, for rock glaciers that move with an average downslope direction along the satellite azimuth direction, the projected velocities could be erroneously high. We found that once the LOS velocities are projected downslope, North Uintas rock glaciers have significantly higher velocities than south Uintas rock glaciers.

InSAR unwrapping errors, which are common in areas with high deformation rates and gradients, also likely introduced inaccuracies in our velocity estimates. Several of the fastest rock glaciers move at rates up to 40 cm/yr in 12 day interferograms, but have velocities < 3 cm/yr in the 1 year pairs used to calculate average velocity. While these discrepancies could be the result of particularly strong seasonal changes in velocity, in longer temporal baseline interferograms, these rock glaciers sometimes had sharp velocity discontinuities consistent with phase jumps caused by unwrapping errors. However, due to the slow velocities of most rock glaciers in the inventory, any unwrapping errors are unlikely to have a large impact on our velocity estimates.

Additional uncertainty in our velocity estimates comes from tropospheric phase delay. We mitigated these errors by 1) estimating velocity using one-year pairs, which results in interferograms with a greater signal-to-noise ratio, 2) averaging multiple high-quality interferograms together and using the stack to estimate velocity, 3) implementing a tropospheric phase delay correction, and 4) choosing local stable reference points. However, due to the large areal extent, large altitudinal range, and highly variable topography of the study region, some non-negligible element of phase delay remains in the one year-stacks we used to estimate velocity (Fig. 2). In general, the descending stack suffered slightly more from atmospheric errors. The uncertainty in the InSAR velocities is unlikely to be systematic in nature as areas of positive and negative velocities appear to be randomly distributed at the elevations where rock glaciers occur. Importantly, the clearly and coherently moving areas of all active or transitional rock glaciers are moving above this level of uncertainty.

5.4 Time-dependent rock glacier deformation

Time series constructed from overlapping sets of interferograms provide insight into how rock glacier velocity varies over three superimposed time scales: 1) seasonal, 2) yearly, and 3) multi-year. Over the four years that we measured displacement, the Grayling Lake, Whiterocks River, and Rockflour Lake rock glaciers displayed continuous motion with no multi-year trend (Fig. 8). It's likely that this observation period was too small to capture possible long-term trends in rock glacier motion, as have been well-documented in the Alps and other regions (Delaloye et al., 2010; Kääb et al., 2007; Kaufmann and Ladstädter, 2007; Roer et al., 2005; Vonder Muehll et al., 2007; Eriksen et al., 2018; Necsoiu et al., 2016).

On the other hand, Uinta rock glaciers do exhibit a significant seasonal velocity pattern. The three representative rock glaciers moved at an average rate of 4.42 cm/yr during the snow-free period from July to October; the rest of the year, they moved at a rate of 0.86 cm/yr. This seasonal rhythm illustrates that Uinta rock glaciers are responsive to the short-term changes in conditions, such as snowmelt.

Examining velocities of individual rock glaciers over time clarifies how they respond to changes in meltwater delivery. For example, the Rockflour Lake rock glacier moved only 0.11 cm in the LOS direction from the winter of 2017/18 to the spring of 2019. While near-zero velocities occurred sporadically for multiple rock glaciers during the snow-covered winter months, the absence of any meaningful acceleration of this rock glacier during the following spring, summer, fall, and winter is unique in our dataset. Spring and summer acceleration in rock glaciers is understood to depend on meltwater and precipitation infiltration to the rock glacier shear zone, increasing pore pressure and decreasing the overall material strength (Wirz et al., 2016; Kenner et al., 2017; Cicoira et al., 2019; Fey and Krainer, 2020). During the winter of 2017/18, snow-water equivalent (SWE) at the Chepeta SNOTEL station, close to the Rockflour Lake rock glacier, was low, and air temperatures were similar to other winters. This correspondence suggests that spring acceleration of Uinta rock glaciers is controlled by snowmelt and that inadequate meltwater infiltration during the spring and summer may cause a rock glacier to effectively "skip" the summer portion of its seasonal cycle. Reduced spring infiltration of liquid water to the shear zone of the Rockflour Lake rock glacier

415   could explain how even as air and ground temperature rose, this feature did not move a measurable distance during the summer
       and fall of 2018.

       Both the Grayling Lake and Whiterocks River rock glaciers accelerated normally during the warmer months of 2018. The
       Grayling Lake rock glacier is close to the Five Points Lake SNOTEL station, which received around 15 cm more SWE than
420   the Chepeta SNOTEL station during the winter of 2017/18 and had a more robust snowmelt event in the spring. Thus, this
       rock glacier likely received the requisite amount of meltwater infiltration for normal acceleration. The Whiterocks River rock
       glacier is closest to the Chepeta SNOTEL station, but is 260 m higher in elevation. Snowpack at the Whiterocks River rock
       glacier may have been much larger than at the Chepeta station, which could explain its normal spring acceleration.
       Alternatively, the Whiterocks River rock glacier could require less water to accelerate in the spring.

425

       Collectively, these results illustrate that Uinta rock glaciers are sensitive to changes in climatic conditions, though individual
       rock glaciers did not respond uniformly to reduced snowmelt in 2018. Our data are not sufficient to determine whether
       dissimilar responses were caused by local variations in climate that weren't reflected in our regional weather data, or by
       individual rock glaciers responding differently to similar climate events. Time series analysis of additional rock glaciers with
430   high-resolution weather data would aid our understanding of Uinta rock glaciers' response to climate events.

5.5 Rock glaciers and climate change

       Our results suggest that Uinta rock glaciers are vulnerable to loss of internal ice due to climate change. Currently, 90.7% of
       these features are found at MAATs above -1.5 °C. If warming continues as predicted, all of these rock glaciers will have
       MAATs at or above 0 °C in the next ten years (IPCC, 2018). Because the PRISM temperature data used here are effectively
435   25 years old, they underestimate current MAATs. PRISM 30 year normals provide a MAAT of 0.11 °C at the Chepeta
       SNOTEL and 0.52 °C at the Five Points Lake SNOTEL, but measured MAAT over the past five years at these stations has
       been warmer, at 1.35 °C and 0.97 °C respectively. It is likely that almost all Uinta rock glaciers are experiencing significant
       ice loss in response to rising temperatures. The presence of 199 inactive rock glaciers supports this claim.

440   Further support for this conclusion comes from the slow velocities of Uinta rock glaciers. In the European Alps and Norway,
       warming temperatures have been associated with rock glacier acceleration and destabilization, as newly established channels
       in permafrost direct meltwater and rain to the shear zone (Delaloye et al., 2010; Kääb et al., 2007; Kaufmann and Ladstädter,
       2007; Roer et al., 2005; Vonder Muehll et al., 2007, Eriksen et al., 2018). However, in these locales, precipitation is generally
       increasing, and rainfall is replacing snowfall. In contrast, at the Five Points Lake and Chepeta SNOTEL station in the Uintas,
445   MAP has decreased over the past 40 years, and rainfall has decreased at a faster rate than snowfall (Fig. 10g, h). In the Uintas,
       and much of the western United States, climate change is characterized by increasing aridity (Gutzler and Robbins, 2011).
       This aridity could explain the slow velocities of Uinta rock glaciers, as 1) reduced winter snowpack means that spring

accelerations are less extreme (Fig. 10a, b), and 2) reduced rainfall results in less heat pumped into the rock glacier interior, and less water in the shear zone, further reducing rock glacier velocity. Thus, rock glacier degradation in the Uintas is unlikely to manifest as destabilization and acceleration. Instead, degrading permafrost may manifest as progressively slower rock glacier velocities and eventual inactivation, as decreasing ice content, increasing frictional interactions from liberated debris, and decreased shear stress as a result of reduced rock glacier thickness serve to slow the rock glacier. These processes can explain the slow velocities of Uinta rock glaciers and may indicate that these features are not as vulnerable to rapid ice loss as those in parts of the world with increasing precipitation and rain. Uinta rock glaciers may, therefore, serve as a water resource for a longer period of time relative to their ice content and are unlikely to undergo hazardous destabilization (Marcer et al., 2021).

5.6 Implications for hydrology

Following calculations in Munroe (2018), which assume a rock glacier and talus thickness of 10 m, an average porosity of 30%, and 25% ice saturation of pore space, active and transitional rock glaciers mapped in this study contain about 1.82×10^7 m^3 of water, equal to about 1% of annual runoff from the Uintas (Jeppson, 1968). Other work has used less conservative numbers for ice content of rock glaciers. For example, Janke et al., (2017) estimated ice content of active rock glaciers in the semiarid Aconcagua River Basin of Chile to be between 25–44.9%, and Jones et al. (2018b) estimated ice content of active rock glaciers in the Nepalese Himalaya to be between 40% and 60%. Using these estimates, active and transitional rock glaciers in the Uintas could store 6.1×10^7–1.46×10^8 m^3 of water, up to 8.10% of the annual runoff from these mountains. These calculations illustrate that rock glaciers in the Uintas could store and seasonally release non-trivial quantities of water. However, if Uinta rock glaciers have experienced significant loss of internal ice due to climate change, water storage will be on the lower end of this spectrum.

While the magnitude of this release may be small compared to the total runoff from the Uintas, it likely makes up a much larger portion of runoff in the high-elevation areas. The timing of meltwater release is also likely to be important. Uinta rock glaciers melt at the fastest rate in the summer, when temperatures are highest, and rainfall delivers liquid water to the interior of the rock glacier. In the late summer, when precipitation in the Uintas is scarce, rock glacier meltwater probably contributes a larger proportion of total streamflow (MacDonald and Tingstad, 2007). As noted by Munroe (2018), if rock glaciers provide a significant input to late summer base flow, climate change will likely produce a short-term increase in water availability, as rock glaciers melt at increased rates, followed by a long-term decrease in water availability (Clow et al. 2003).

6 Conclusions

In this study an inventory of 205 active and transitional rock glaciers in the Uinta Mountains, Utah was constructed using InSAR from the Copernicus Sentinel-1 satellites, Google Earth imagery, and topographic data. Rock glaciers in the Uinta Mountains have an average area of 11.9 ha, commonly face north or northeast, and are found within a narrow elevation band

480 ranging from 3100 and 3500 (average of 3290 m), corresponding to a MAAT of 0.5 to -2.0° C (average of -0.15° C). Rock glacier location is controlled by a combination of mountain geometry and air temperature. InSAR-derived downslope rock glacier velocities are between 0.35 and 6.03 cm/yr, with an average of 1.92 cm/yr, and are not correlated with variables including elevation, area, aspect, slope, or morphology. Time series analysis of three rock glaciers revealed a seasonal rhythm in LOS velocities, with an average of 4.42 cm/yr during the snow-free late summer, and 0.86 cm/yr during the rest of the year.

485 The Rockflour Lake rock glacier did not accelerate during 2018 because of minimal spring snowmelt following a winter with abnormally low snowfall. We speculate that generally slow rock glacier velocities throughout the Uintas may be related to reduced ice content and increasing aridity caused by ongoing climate change. We estimate that rock glaciers in the Uintas store a volume of water equivalent to 1-9% of annual runoff from these mountains. During the late summer, when precipitation over the Uintas is comparatively low, rock glacier melting may provide an important addition to stream base flow, particularly at

490 high elevations. As climate change continues, the rock glacier contribution to late summer runoff is expected to increase, as rock glaciers melt, before decreasing in the long term, as Uinta rock glaciers become relict.

Data Availability

The research data used in this study are freely available online. SAR scenes used to generate interferograms are available on

495 the Alaska Satellite Foundation Vertex website (https://vertex.daac.asf.alaska.edu/). Corresponding POD Precise Orbit Ephemerides data can be found on the ESA website (https://scihub.copernicus.eu/gnss/#/home). The 30 m SRTM DEM is available from the USGS Earth Explorer website (https://earthexplorer.usgs.gov/), and the 10 m USGS 3DEP DEM is available from the USGS National Map website (https://viewer.nationalmap.gov/basic/). PRISM data can be downloaded from the PRISM website (https://prism.oregonstate.edu/). SNOTEL data are available on the Natural Resources Conservation Service

500 website (https://www.nrcs.usda.gov/wps/portal/wcc/home/).

Author Contribution

J.M. and A.H. devised the idea for the project. A.H. and G.B. designed the methodology. G.B. carried out the methodology with guidance from A.H. G.B. analysed the data. G.B. made the figures with advice from J.M. and A.H. G.B. wrote the

505 manuscript with significant input from J.M. and A.H.

Conflicts of Interest

The authors declare that they have no conflict of interest.

510 **Acknowledgements**

Funding was provided by National Science Foundation award EAR-1935200 to A. Handwerger and J. Munroe. Part of this research was carried out at the Jet Propulsion Laboratory, California Institute of Technology, under a contract with the National

Aeronautics and Space Administration (80NM0018D0004). We'd like to thank the scientists at the Jet Propulsion Laboratory for generously providing their insight to G.B. during a research visit. Funding to support the JPL visit was awarded to G.B. by
515   Middlebury College's Senior Research Project Supplement.

References

Arenson, L., Hoelzle, M., and Springman, S.: Borehole deformation measurements and internal structure of some rock glaciers in Switzerland, Permafr. Periglac. Process., 13(2), 117–135, https://doi.org/10.1002/ppp.414, 2002.

520   Azócar, G., and Brenning, A.: Hydrological and geomorphological significance of rock glaciers in the dry Andes, Chile (27–33 S), Permafr. Periglac. Process., 21(1), 42–53, https://doi.org/10.1002/ppp.669, 2010.

Barboux, C., Delaloye, R., and Lambiel, C.: Inventorying slope movements in an Alpine environment using DInSAR. Earth Surf. Process. Landf, 39(15), 2087-2099, https://doi.org/10.1002/esp.3603, 2014.

525

Barnett, T. P., and Pierce, D. W.: When will Lake Mead go dry?, Water Resour. Res., 44(3), W03201, https://doi.org/10.1029/2007WR006704, 2008.

Barsch, D.: Rock-glaciers: Indicators for the present and former geoecology of high mountain environments. Springer, Berlin
530   Heidelberg, Germany, 1996.

Bayer, B., Simoni, A., Mulas, M., Corsini, A., and Schmidt, D.: Deformation responses of slow moving landslides to seasonal rainfall in the Northern Apennines, measured by InSAR, Geomorphology, 308, 293–306, https://doi.org/10.1016/j.geomorph.2018.02.020, 2018.

535

Bekaert, D. P. S., Walters, R. J., Wright, T. J., Hooper, A. J., and Parker, D. J.: Statistical comparison of InSAR tropospheric correction techniques, Remote Sens. Environ., 170, 40–47, https://doi.org/10.1016/j.rse.2015.08.035, 2015.

Berardino, P., Fornaro, G., Lanari, R., and Sansosti, E.: A new algorithm for surface deformation monitoring based on small
540   baseline differential SAR interferograms. IEEE Trans. Geosci. Remote Sens., 40(11), 2375–2383, https://doi.org/10.1109/TGRS.2002.803792, 2002.

Boeckli, L., Brenning, A., Gruber, S., and Noetzli, J.: Permafrost distribution in the European Alps: calculation and evaluation of an index map and summary statistics, Cryosphere, 6(4), 807–820, https://doi.org/10.5194/tc-6-807-2012, 2012.

Bradley, W.H.: Geomorphology of the North Flank of the Uinta Mountains, US Geological Survey, US Government Printing Office, Washington DC, USA, https://doi.org/10.3133/pp185I, 1936.

Brardinoni, F., Scotti, R., Sailer, R., and Mair, V.: Evaluating sources of uncertainty and variability in rock glacier inventories, Earth Surf. Process. Landf., 44, 2450–2466, https://doi.org/10.1002/esp.4674, 2019.

Chen, C. W., and Zebker, H. A.: Phase unwrapping for large SAR interferograms: Statistical segmentation and generalized network models, IEEE Trans. Geosci. Remote. Sens., 40(8), 1709–1719, https://doi.org/ 10.1109/TGRS.2002.802453, 2002.

Cicoira, A., Beutel, J., Faillettaz, J., and Vieli, A.: Water controls the seasonal rhythm of rock glacier flow, Earth Planet. Sci. Lett., 528, 115844, https://doi.org/10.1016/j.epsl.2019.115844, 2019.

Clow, D. W., Schrott, L., Webb, R., Campbell, D. H., Torizzo, A., and Dornblaser, M.: Ground water occurrence and contributions to streamflow in an alpine catchment, Colorado Front Range, Groundwater, 41(7), 937–950, https://doi.org/10.1111/j.1745-6584.2003.tb02436.x, 2003.

Degenhardt Jr, J. J.: Development of tongue-shaped and multilobate rock glaciers in alpine environments–Interpretations from ground penetrating radar surveys. Geomorphology, 109(3–4), 94–107, https://doi.org/10.1016/j.geomorph.2009.02.020, 2009.

Dehler, C.M., Porter, S.M., De Grey, L.D., Sprinkel, D.A., and Brehm, A.: The Neoproterozoic Uinta Mountain Group revisited; a synthesis of recent work on the Red Pine Shale and related undivided clastic strata, northeastern Utah, U.S.A., In Proterozoic Geology of Western North America and Siberia, Link, P. K., Lewis, R. S., Society for Sedimentary Geology, Tulsa, USA, 151–166, https://doi.org/10.2110/pec.07.86.0151, 2007.

Delaloye, R., Lambiel, C., and Gärtner-Roer, I.: Overview of rock glacier kinematics research in the Swiss Alps: seasonal rhythm, interannual variations and trends over several decades, Geogr. Helv., 65(2), 135–145, https://doi.org/10.5194/gh-65-135-2010, 2010.

Eriksen, H. Ø., Rouyet, L., Lauknes, T. R., Berthling, I., Isaksen, K., Hindberg, H., Larsen, Y., and Corner, G. D.: Recent acceleration of a rock glacier complex, Adjet, Norway, documented by 62 years of remote sensing observations, Geophys. Res. Lett., 45(16), 8314–8323, https://doi.org/10.1029/2018GL077605, 2018.

580

Falaschi, D., Castro, M., Masiokas, M., Tadono, T., and Ahumada, A. L.: Rock glacier inventory of the Valles Calchaquíes region (~ 25 S), Salta, Argentina, derived from ALOS data, Permafr. Periglac. Process., 25(1), 69–75, https://doi.org/10.1002/ppp.1801, 2014.

585 Fey, C., and Krainer, K.: Analyses of UAV and GNSS based flow velocity variations of the rock glacier Lazaun (Ötztal Alps, South Tyrol, Italy), Geomorphology, 365, 107261, https://doi.org/10.1016/j.geomorph.2020.107261, 2020.

Frauenfelder, R., and Kääb, A.: Towards a palaeoclimatic model of rock-glacier formation in the Swiss Alps, Ann. Glaciol., 31, 281–286, https://doi.org/10.3189/172756400781820264, 2000.

590

Gutzler, D. S., and Robbins, T. O.: Climate variability and projected change in the western United States: regional downscaling and drought statistics, Clim. Dyn., 37(5–6), 835–849, https://doi.org/ 10.1007/s00382-010-0838-7, 2011.

Haeberli, W.: Creep of mountain permafrost: internal structure and flow of alpine rock glaciers, Mitteilungen der
595   Versuchsanstalt fur Wasserbau, Hydrologie und Glaziologie an der ETH Zurich, 77, 1985.

Haeberli, W., Hallet, B., Arenson, L., Elconin, R., Humlum, O., Kääb, A., Kaufmann, V., Ladanyi, B., Matsuoka, N., Springman, S., and Mühll, D. V.: Permafrost creep and rock glacier dynamics, Permafr. Periglac. Process., 17(3), 189–214, https://doi.org/10.1002/ppp.561, 2006.

600

Hales, T. C., and Roering, J. J.: Climatic controls on frost cracking and implications for the evolution of bedrock landscapes, J. Geophys. Res. Earth Surf., 112(F2), https://doi.org/10.1029/2006JF000616, 2007.

Handwerger, A. L., Fielding, E. J., Huang, M. H., Bennett, G. L., Liang, C., and Schulz, W. H.: Widespread initiation,
605   reactivation, and acceleration of landslides in the northern California Coast Ranges due to extreme rainfall, J. Geophys. Res. Earth Surf., 124(7), 1782–1797, https://doi.org/10.1029/2019JF005035, 2019.

Hinzman, L. D., Goering, D. J., and Kane, D. L.: A distributed thermal model for calculating soil temperature profiles and depth of thaw in permafrost regions, J. Geophys. Res. Atmos., 103(D22), 28975–28991,
610   https://doi.org/10.1029/98JD01731, 1998.

Hoelzle, M., and Haeberli, W.: Simulating the effects of mean annual air-temperature changes on permafrost distribution and glacier size: an example from the Upper Engadin, Swiss Alps, Ann. Glaciol., 21, 399–405, https://doi.org/10.3189/S026030550001613X, 1995.

615

Ikeda, A., Matsuoka, N., and Kääb, A.: Fast deformation of perennially frozen debris in a warm rock glacier in the Swiss Alps: An effect of liquid water, J. Geophys. Res. Earth Surf., 113(F1), https://doi.org/10.1029/2007JF000859, 2008.

IPA Action Group Rock Glacier Inventories and Kinematics: Baseline Concepts Version 4.1. Université de Fribourg

620   Geomorphology Research Group, https://www.unifr.ch/geo/geomorphology/en/research/ipa-action-group-rock-glacier/, 2020.

IPCC: Summary for Policymakers. In Global Warming of 1.5°C. An IPCC Special Report on the impacts of global warming of 1.5°C above pre-industrial levels and related global greenhouse gas emission pathways, in the context of

625   strengthening the global response to the threat of climate change, sustainable development, and efforts to eradicate poverty, Masson-Delmotte, V., Zhai, P., Pörtner, H. O., Roberts, D., Skea, J., Shukla, P. R., Pirani, A., Moufouma-Okia, W., Péan, C., Pidcock, R., Connors, S., Matthews, J. B. R., Chen, Y., Zhou, X., Gomis, M. I., Lonnoy, E., Maycock, T., Tignor, M., and Waterfield, T., World Meteorological Organization, Geneva, Switzerland, 32 pp, 2018.

630 Janke, J. R.: Long-term flow measurements (1961–2002) of the Arapaho, Taylor, and Fair rock glaciers, Front Range, Colorado, Phys. Geogr., 26(4), 313–336, https://doi.org/10.2747/0272-3646.26.4.313, 2005.

Janke, J. R.: Colorado Front Range rock glaciers: distribution and topographic characteristics, Arct. Antarct. Alp. Res., 39(1), 74–83, https://doi.org/10.1657/1523-0430(2007)39[74:CFRRGD]2.0.CO;2, 2007.

635

Janke, J. R., Ng, S., and Bellisario, A.: An inventory and estimate of water stored in firn fields, glaciers, debris-covered glaciers, and rock glaciers in the Aconcagua River Basin, Chile, Geomorphology, 296, 142–152, https://doi.org/10.1016/j.geomorph.2017.09.002, 2017.

640 Jeppson, R. W.: Hydrologic Atlas of Utah, Utah Water Research Laboratory, Utah State University, Logan, USA, Paper 297, https://digitalcommons.usu. edu/water_rep/297, 1968.

Johnson, B. G., Thackray, G. D., and Van Kirk, R.: The effect of topography, latitude, and lithology on rock glacier distribution in the Lemhi Range, central Idaho, USA, Geomorphology, 91(1-2), https://doi.org/10.1016/j.geomorph.2007.01.023,
645   38-50, (2007).

Jones, D. B., Harrison, S., Anderson, K., and Betts, R. A.: Mountain rock glaciers contain globally significant water stores, Sci. Rep., 8(1), 2834, https://doi.org/10.1038/s41598-018-21244-w, 2018a.

650   Jones, D. B., Harrison, S., Anderson, K., Selley, H. L., Wood, J. L., and Betts, R. A.: The distribution and hydrological significance of rock glaciers in the Nepalese Himalaya, Glob. Planet. Change, 160, 123–142, https://doi.org/10.1016/j.gloplacha.2017.11.005, 2018b.

Kääb, A., Frauenfelder, R., and Roer, I.: On the response of rockglacier creep to surface temperature increase, Glob. Planet.
655   Change, 56(1–2), 172–187, https://doi.org/10.1016/j.gloplacha.2006.07.005, 2007.

Kääb, A., Strozzi, T., Bolch, T., Caduff, R., Trefall, H., Stoffel, M., & Kokarev, A: Inventory and changes of rock glacier creep speeds in Ile Alatau and Kungöy Ala-Too, northern Tien Shan, since the 1950s. The Cryosphere, 15(2), 927-949, https://doi.org/10.5194/tc-15-927-2021. 2021.

660   Kaufmann, V., and Ladstädter, R.: Mapping of the 3D surface motion field of Doesen rock glacier (Ankogel group, Austria) and its spatio-temporal change (1954–1998) by means of digital photogrammetry, In International Symposium on High Mountain Remote Sensing Cartography, 127–144, 2007

Kellerer-Pirklbauer, A., Lieb, G. K., and Kleinferchner, H.: A new rock glacier inventory of the eastern European Alps,
665   Austrian J. Earth Sci., 105(2), 2012.

Kenner, R., Phillips, M., Beutel, J., Hiller, M., Limpach, P., Pointner, E., and Volken, M.: Factors controlling velocity variations at short-term, seasonal and multiyear time scales, Ritigraben rock glacier, Western Swiss Alps, Permafr. Periglac. Process., 28(4), 675–684, https://doi.org/10.1002/ppp.1953, 2017.

670

Kenyi, L. W., and Kaufmann, V.: Estimation of rock glacier surface deformation using SAR interferometry data, IEEE Trans. Geosci. Remote. Sens., 41(6), 1512–1515, https://doi.org/10.1109/TGRS.2003.811996, 2003.

Krainer, K., and Ribis, M.: A rock glacier inventory of the Tyrolean Alps (Austria), Austrian J. Earth Sci., 105(2), 2012.
675

Lieb, G.K.: Permafrost und Blockgletscher in den östlichen österreichischen Alpen, Arbeiten aus dem Institut für Geographie der Karl-Franzens-Universität Graz, Band 33, 9–125, 1996.

Lilleøren, K. S., and Etzelmüller, B.: A regional inventory of rock glaciers and ice-cored moraines in Norway, Geogr. Ann. A: Phys. Geogr., 93(3), 175–191, https://doi.org/10.1111/j.1468-0459.2011.00430.x, 2011.

Lilleøren, K. S., Etzelmüller, B., Gärtner-Roer, I., Kääb, A., Westermann, S., and Guðmundsson, Á.: The distribution, thermal characteristics and dynamics of permafrost in Tröllaskagi, northern Iceland, as inferred from the distribution of rock glaciers and ice-cored moraines, Permafr. Periglac. Process., 24(4), 322–335, https://doi.org/10.1002/ppp.1792, 2013.

Liu, L., Millar, C. I., Westfall, R. D., and Zebker, H. A.: Surface motion of active rock glaciers in the Sierra Nevada, California, USA: inventory and a case study using InSAR, Cryosphere, 7, 1109–1119, https://doi.org/10.5194/tc-7-1109-2013, 2013.

Luckman, B. H., and Crockett, K. J.: Distribution and characteristics of rock glaciers in the southern part of Jasper National Park, Alberta. Can. J. Earth Sci., 15(4), 540-550, https://doi.org/10.1139/e78-060, 1978.

MacDonald, G. M., and Tingstad, A. H.: Recent and multicentennial precipitation variability and drought occurrence in the Uinta Mountains region, Utah, Arct. Antarct. Alp. Res., 39(4), 549–555, https://doi.org/10.1657/1523-0430(06-070), 2007.

Marcer, M., Cicoira, A., Cusicanqui, D., Bodin, X., Echelard, T., Obregon, R., & Schoeneich, P: Rock glaciers throughout the French Alps accelerated and destabilised since 1990 as air temperatures increased. Communications Earth & Environment, 2(1), 1-11. https://doi.org/10.1038/s43247-021-00150-6. 2021

Moore, P. L.: Deformation of debris-ice mixtures, Rev. Geophys., 52(3), 435–467, https://doi.org/10.1002/2014RG000453, 2014.

Müller, J., Vieli, A., and Gärtner-Roer, I.: Rock glaciers on the run–understanding rock glacier landform evolution and recent changes from numerical flow modelling, Cryosphere, 10(6), 2865–2886, https://doi.org/10.5194/tc-10-2865-2016, 2016.

Munroe, J. S.: Distribution, evidence for internal ice, and possible hydrologic significance of rock glaciers in the Uinta Mountains, Utah, USA, Quat. Res., 90(1), 50–65, https://doi.org/10.1017/qua.2018.24, 2018.

710

Munroe, J. S., and Laabs, B. J. C.: Glacial Geologic Map of the Uinta Mountains Area, Utah and Wyoming, Utah Geological Survey Miscellaneous Publication, Utah Geological Survey, Salt Lake City, USA, 2009.

Nagler, T., Mayer, C., and Rott, H.: Feasibility of DINSAR for mapping complex motion fields of Alpine ice-and rock-glaciers,

715 In Retrieval of Bio-and Geo-Physical Parameters from SAR Data for Land Applications, 475, 377–382, 2002.

Necsoiu, M., Onaca, A., Wigginton, S., and Urdea, P.: Rock glacier dynamics in Southern Carpathian Mountains from high-resolution optical and multi-temporal SAR satellite imagery, Remote Sens. Environ., 177, 21-36, https://doi.org/10.1016/j.rse.2016.02.025, 2016.

720

Nicholson, L., Marín, J., Lopez, D., Rabatel, A., Bown, F., and Rivera, A.: Glacier inventory of the upper Huasco valley, Norte Chico, Chile: glacier characteristics, glacier change and comparison with central Chile, Ann. Glaciol., 50(53), 111–118, https://doi.org/10.3189/172756410790595787, 2009.

725 Perruchoud, E., and Delaloye, R.: Short-Term Changes in Surface Velocities on the Becs-de-Bosson Rock Glacier (Western Swiss Alps), Grazer Schriften der Geographie und Raumforschung, 43, 2007.

Rangecroft, S., Harrison, S., Anderson, K., Magrath, J., Castel, A. P., and Pacheco, P.: A first rock glacier inventory for the Bolivian Andes, Permafr. Periglac. Process., 25(4), 333–343, https://doi.org/10.3189/10.1002/ppp.1816, 2014.

730

Rempel, A. W., Marshall, J. A., and Roering, J. J.: Modeling relative frost weathering rates at geomorphic scales, Earth Planet. Sci. Lett., 453, 87–95, https://doi.org/10.1016/j.epsl.2016.08.019, 2016.

Rick, B., Delaloye, R., Barboux, C., and Strozzi, T.: Detection and inventorying of slope movements in the Brooks Range, 735 Alaska using DInSAR: a test study, In proceedings of the GEOQuébec 2015: 68th Canadian Geotechnical Conference and 7th Canadian Permafrost Conference, 2015.

Rignot, E., Hallet, B., and Fountain, A.: Rock glacier surface motion in Beacon Valley, Antarctica, from synthetic-aperture radar interferometry, Geophys. Res. Lett., 29(12), 48-1–48-4, https://doi.org/10.1029/2001GL013494, 2002.

740

Roer, I., Kääb, A., and Dikau, R.: Rockglacier acceleration in the Turtmann valley (Swiss Alps): Probable controls, Nor. J. Geogr., 59(2), 157–163, https://doi.org/10.1080/00291950510020655, 2005.

Rosen, P. A., Gurrola, E., Sacco, G. F., and Zebker, H.: The InSAR scientific computing environment, In 9th European Conference on Synthetic Aperture Radar, Nuremberg, Germany, 730–733, 2012.

Roudnitska, S., Charvet, R., Ribeyre, C., and Favreaux, B. L. Les Glaciers-Rocheux De Savoie: Inventaire, Cartographie Et Risques Associés - Rapport Provisoire, Chambery: Office National des Forets, Service de Restauration des Terrains en Montagne, 2016.

Schaffer, N., MacDonell, S., Réveillet, M., Yáñez, E., and Valois, R.: Rock glaciers as a water resource in a changing climate in the semiarid Chilean Andes, Reg. Environ. Change, 1–17, https://doi.org/10.1007/s10113-018-01459-3, 2019.

Schmidt, D. A., and Bürgmann, R.: Time-dependent land uplift and subsidence in the Santa Clara valley, California, from a large interferometric synthetic aperture radar data set, J. Geophys. Res. Solid Earth, 108(B9), https://doi.org/10.1029/2002JB002267, 2003.

Schmid, M. O., Baral, P., Gruber, S., Shahi, S., Shrestha, T., Stumm, D., and Wester, P.: Assessment of permafrost distribution maps in the Hindu Kush Himalayan region using rock glaciers mapped in Google Earth, Cryosphere, 9(6), 2089–2099, https://doi.org/10.5194/tcd-8-5293-2014, 2015.

Sears, J. W., Graff, P. J., and Holden, G. S.: Tectonic evolution of lower Proterozoic rocks, Uinta Mountains, Utah and Colorado, Geol. Soc. Am. Bull., 93(10), 990–997, https://doi.org/10.1130/0016-7606(1982)93<990:TEOLPR>2.0.CO;2, 1982.

Strozzi, T., Kääb, A., and Frauenfelder, R.: Detecting and quantifying mountain permafrost creep from in situ inventory, space-borne radar interferometry and airborne digital photogrammetry, Int. J. Remote Sens., 25(15), 2919-2931, https://doi.org/10.1080/0143116042000192330, 2004.

Strozzi, T., Caduff, R., Jones, N., Barboux, C., Delaloye, R., Bodin, X., ... & Schrott, L: Monitoring rock glacier kinematics with satellite synthetic aperture radar. Remote Sensing, 12(3), 559, https://doi.org/10.3390/rs12030559, 2020.

Tingstad, A. H.: Climate variability and ecological response in the Uinta Mountains, Utah, inferred from diatoms and tree-rings, PhD thesis, University of California, Los Angeles, USA, 2010.

Villarroel, C., Tamburini Beliveau, G., Forte, A., Monserrat, O., and Morvillo, M.: DInSAR for a regional inventory of active rock glaciers in the dry Andes Mountains of Argentina and Chile with Sentinel-1 data, Remote Sensing, 10(10), 1588, https://doi.org/10.3390/rs10101588, 2018.

Vonder Mühll, D., Noetzli, J., Roer, I., Makowski, K., and Delaloye, R.: Permafrost in Switzerland 2002/2003 and
780   2003/2004, Glaciological Report (Permafrost) No, 4(5), 2007.

Wahrhaftig, C., and Cox, A.: Rock glaciers in the Alaska Range, Geol. Soc. Am. Bull., 70(4), 383–436,
        https://doi.org/10.1130/0016-7606(1959)70[383:RGITAR]2.0.CO;2, 1959.

785 Wang, X., Liu, L., Zhao, L., Wu, T., Li, Z., and Liu, G.: Mapping and inventorying active rock glaciers in the northern Tien
        Shan of China using satellite SAR interferometry, Cryosphere, 11(2), 997–1014, https://doi.org/10.5194/tc-11-997-
        2017, 2017.

Wirz, V., Gruber, S., Purves, R. S., Beutel, J., Gärtner-Roer, I., Gubler, S., and Vieli, A.: Short-term velocity variations at
790   three rock glaciers and their relationship with meteorological conditions, Earth Surf. Dyn., 4(1), 103–123,
        https://doi.org/10.5194/esurf-4-103-2016, 2016.

Zasadni, J., and Kłapyta, P.: From valley to marginal glaciation in alpine-type relief: Late glacial glacier advances in the Pięć
        Stawów Polskich/Roztoka Valley, High Tatra Mountains, Poland, Geomorphology, 253, 406–424,
795   https://doi.org/10.1016/j.geomorph.2015.10.032, 2016.
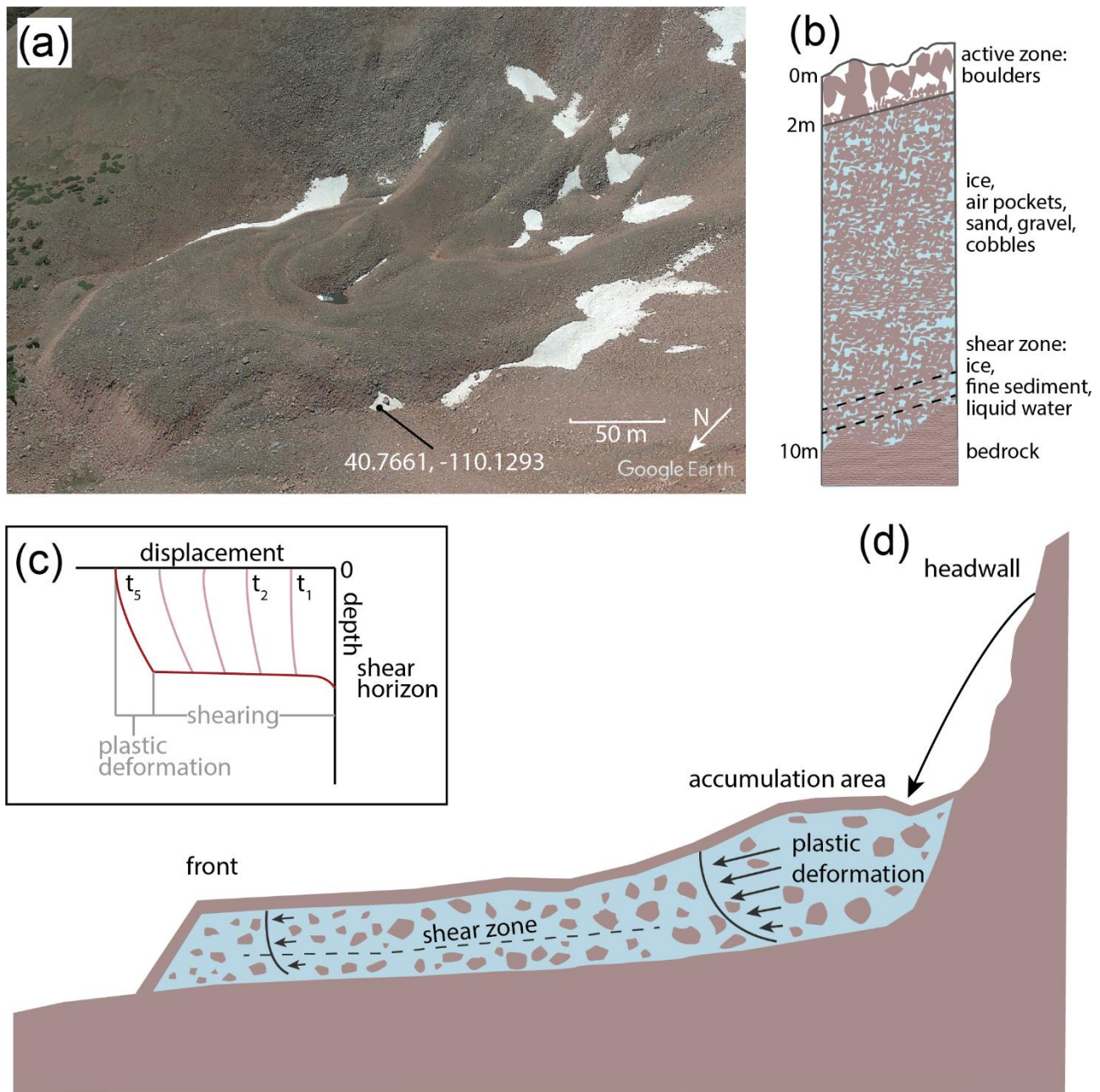
Figure 1. Figure showing general internal structure and deformation of rock glaciers. (a) Oblique view of a Uinta Mountain rock glacier from © Google Earth. (b) Schematic stratigraphic cross section of a rock glacier in the Uinta Mountains. Schematic diagram is based on borehole data from Arenson et al. (2002). (c) Plot showing how total displacement is related to shearing and plastic deformation in rock glaciers. Deformation primarily occurs along shear horizons within rock glaciers. (d) Schematic showing rock glacier deformation ((c) and (d) after Kenner et al. 2017).
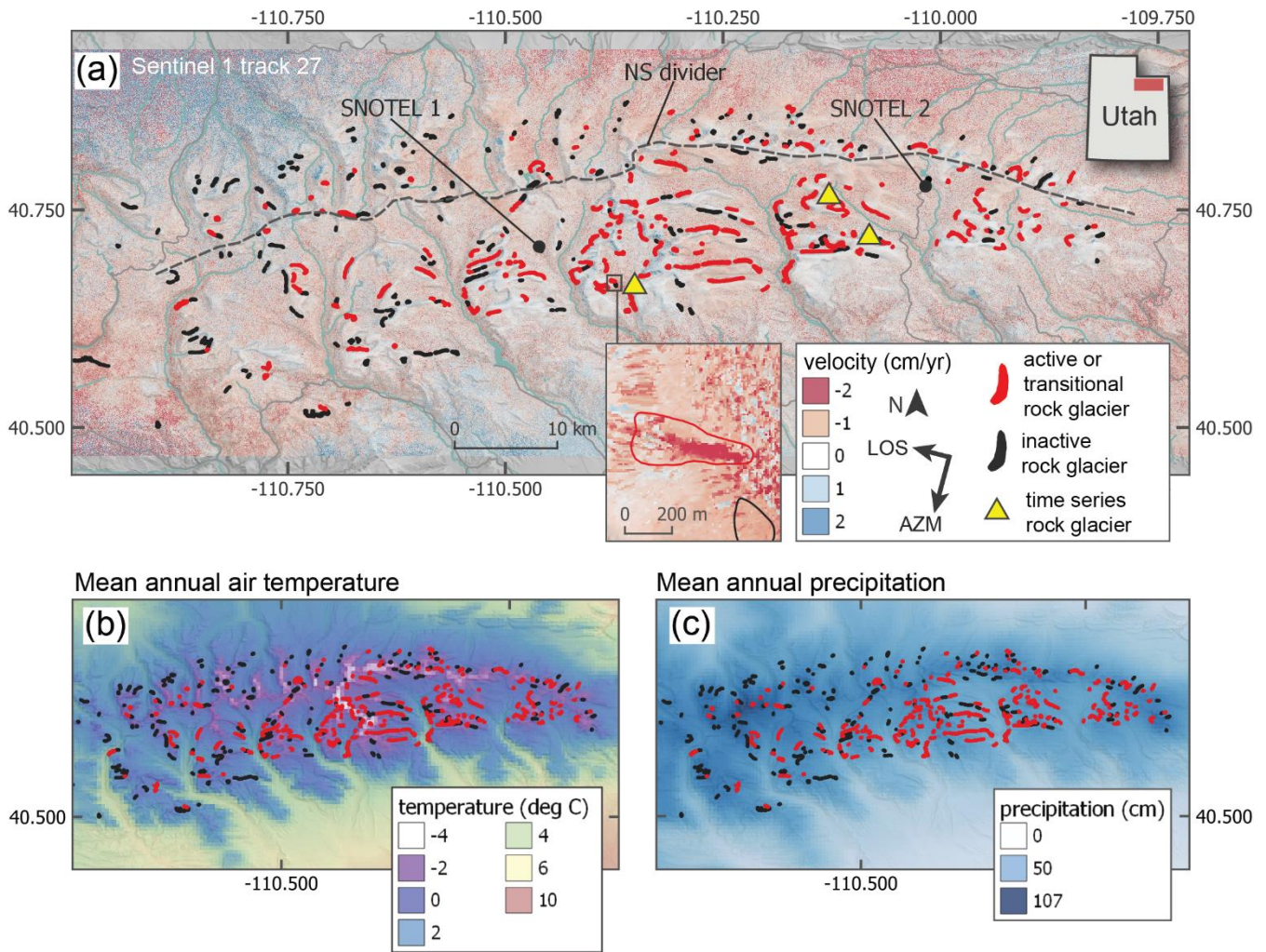
Figure 2. Uinta Mountains study site. (a) Hillshade map of the Uinta Mountains overlaid with average one-year InSAR velocity map derived from descending track 27. Red polygons represent active rock glaciers identified in this study. Black polygons represent rock glaciers identified in the previous inventory (Munroe, 2018) which are inactive (i.e., show no coherent and distinct deformation) in our InSAR velocity maps. Rock glacier size is exaggerated for plotting. SNOTEL 1 is the Five Points Lake station. SNOTEL 2 is the Chepeta station. The black dashed line separates the "North Uintas" from the "South Uintas". Yellow triangles represent the three rock glaciers used in time series analysis, which are, from left to right, the Grayling Lake, Whiterocks River, and Rockflour Lake rock glaciers. Data from USGS, NRCS, and Natural Earth. (b) Mean annual air temperature of the Uinta Mountains. (c) Mean annual precipitation in the Uinta Mountains. In (b) and (c), data are derived from PRISM 30 year normals (1981-2010).
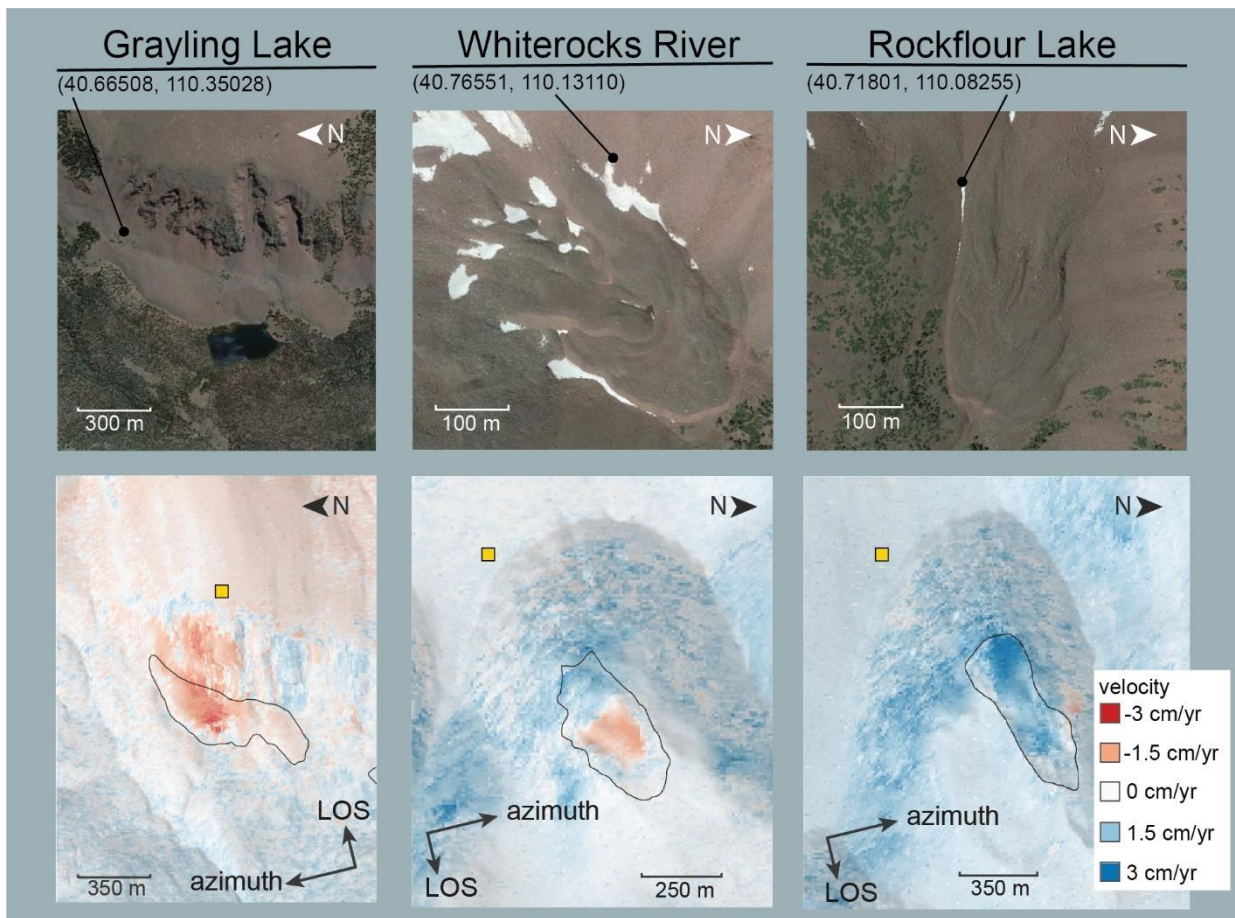
Figure 3. Individual rock glaciers investigated with time series. (top) Overhead view of rock glaciers in © Google Earth, annotated in Adobe Illustrator. (bottom) Average velocity stack draped over a hillshade. Rock glaciers were added to our active inventory if they displayed clear deformation signal, like those above. Yellow squares represent stable local reference points used in our time series analysis.
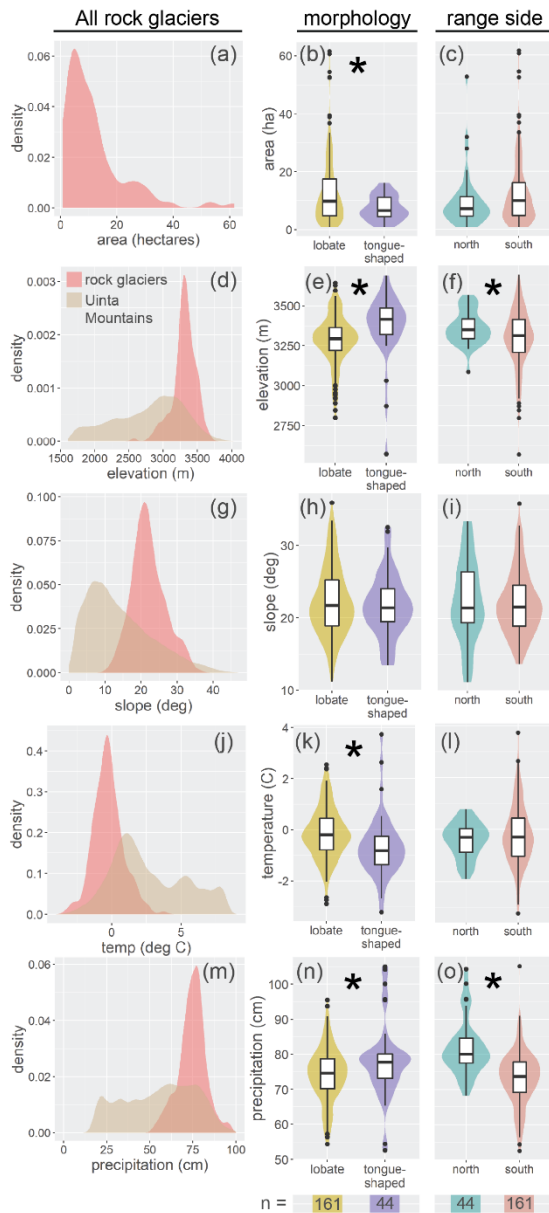
Figure 4. Characteristics of active rock glaciers in the Uinta Mountains. Slope, area, and elevation were calculated using the rock glacier inventory polygons and a DEM in QGIS. Temperature and precipitation were calculated using the rock glacier inventory polygons and PRISM data in QGIS. (a, d, g, j, m) Data for all rock glaciers and the Uinta Mountains shown as kernel density plots. (b, c, e, f, h, i, k, l, n, o) Colored violin plots on the right show rock glacier characteristics based on morphology and location within the Uintas. Asterisks denote statistically significant differences. n = 205.
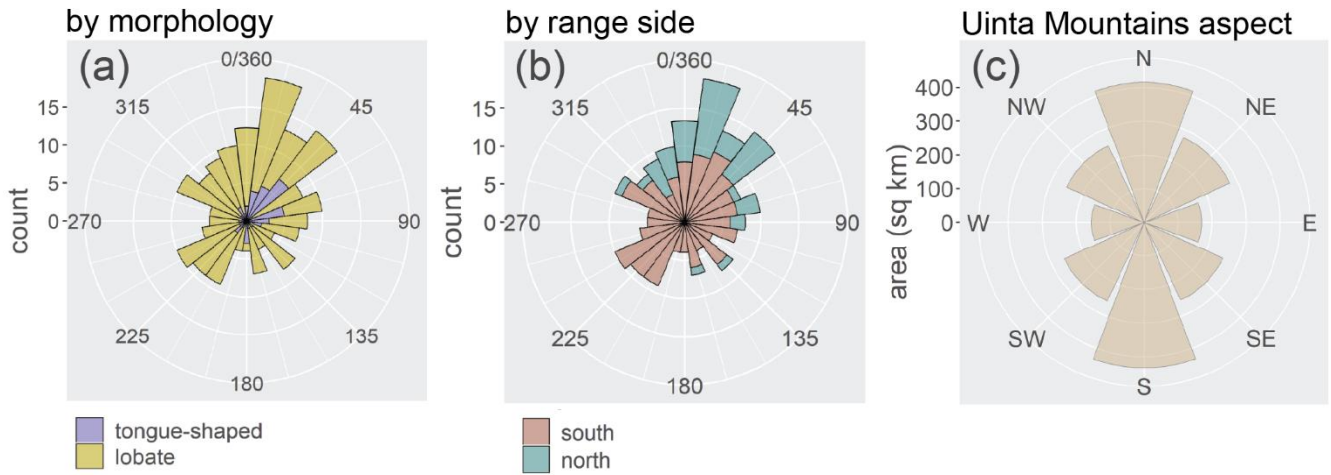
Figure 5. Polar plots showing aspect of active rock glaciers from the Uinta Mountains inventory and aspect of the steep slopes (>10˚) of the Uinta Mountains. (a) Aspect is classified by rock glacier morphology. (b) Aspect is classified by which side of the Uinta Mountains the rock glacier is on. (c) Aspect of steep slopes (>10˚) of the Uinta Mountains, for reference. Data are
835   derived from rock glacier inventory polygons and a USGS DEM.
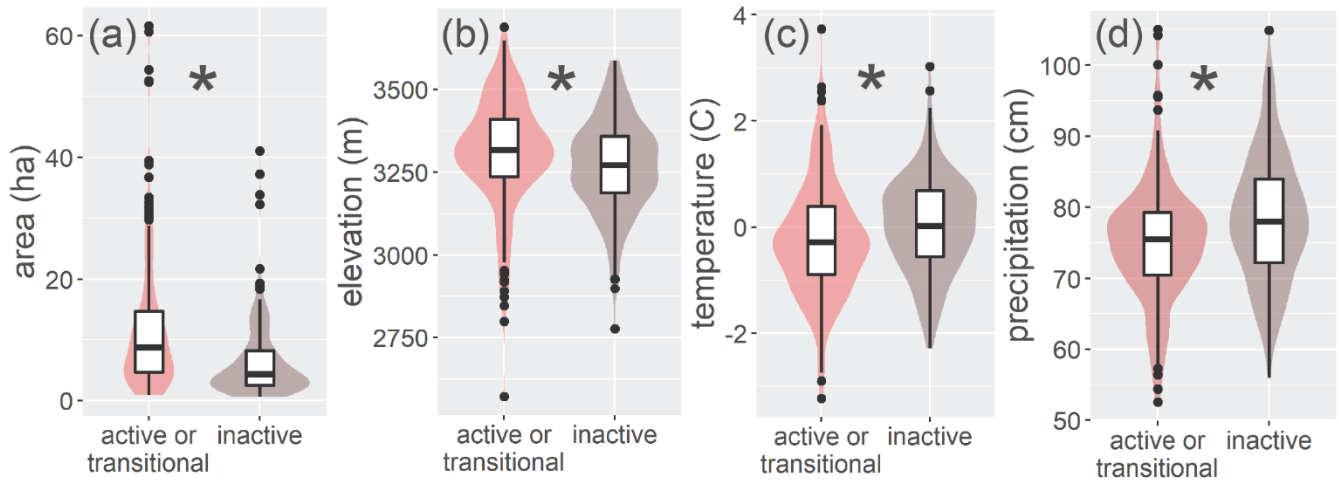
Figure 6. Violin plots comparing active rock glaciers with inactive rock glaciers from the previous Uinta rock glaciers
840   inventory. Asterisks denote statistically significant differences. n = 404
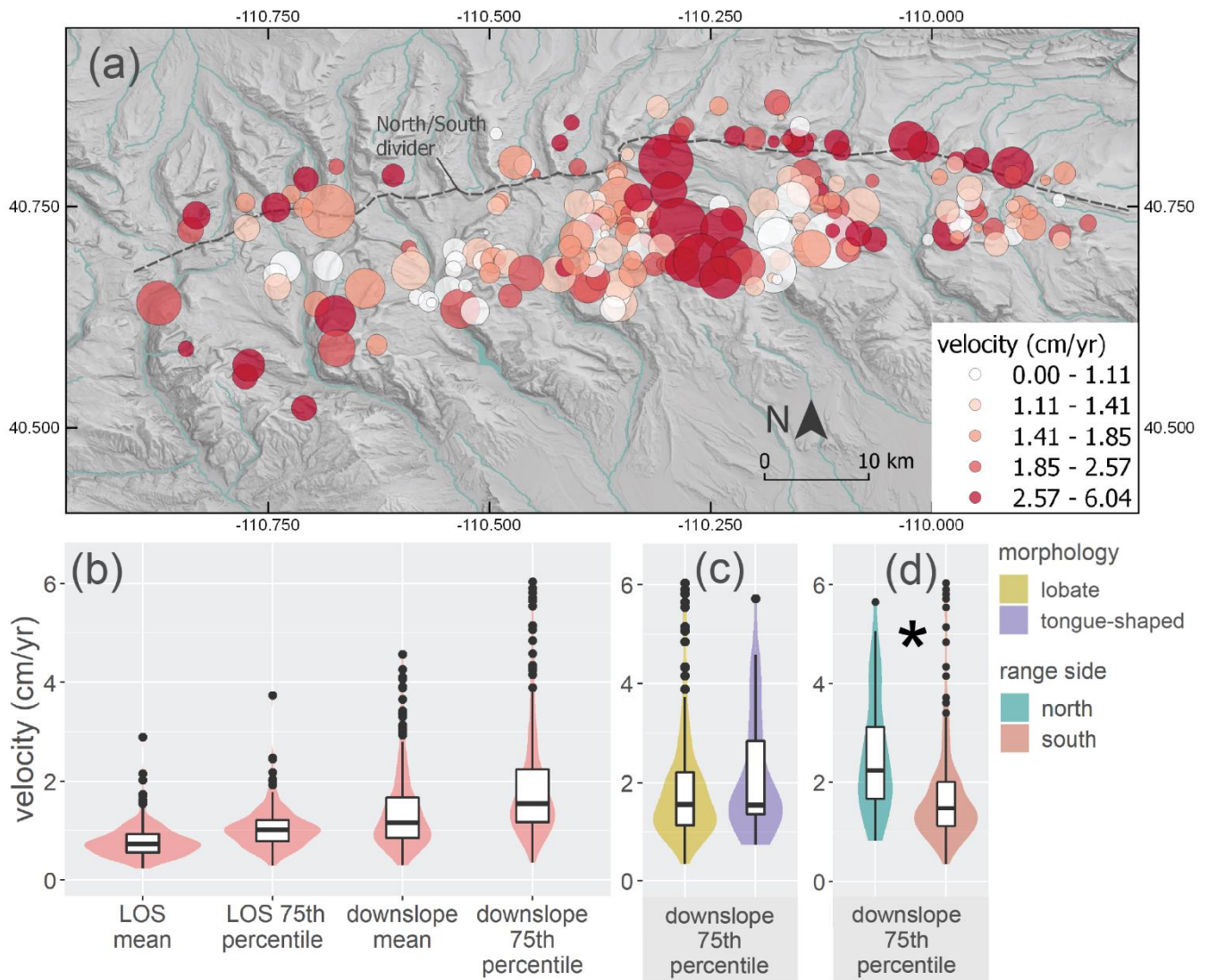
Figure 7. Average annual downslope velocity of active Uinta rock glaciers from 2016-2019. (a) Map showing rock glacier
845   area and velocity. Each rock glacier is represented by a circle. Size of circle represents relative rock glacier area and color
represents absolute value of rock glacier 75th percentile downslope velocity. Note fewer, smaller, slower rock glaciers in the
North Uintas. (b) Violin plots show absolute value of mean and 75th percentile LOS and downslope velocities for all rock
glaciers. (c) Violin plots show 75th percentile downslope velocities for rock glaciers classified by morphology. (d) Violin plots
show 75th percentile downslope velocities for rock glaciers classified by which side of the Uinta Mountains they are on.
850   Asterisks denote significant differences. n = 205.
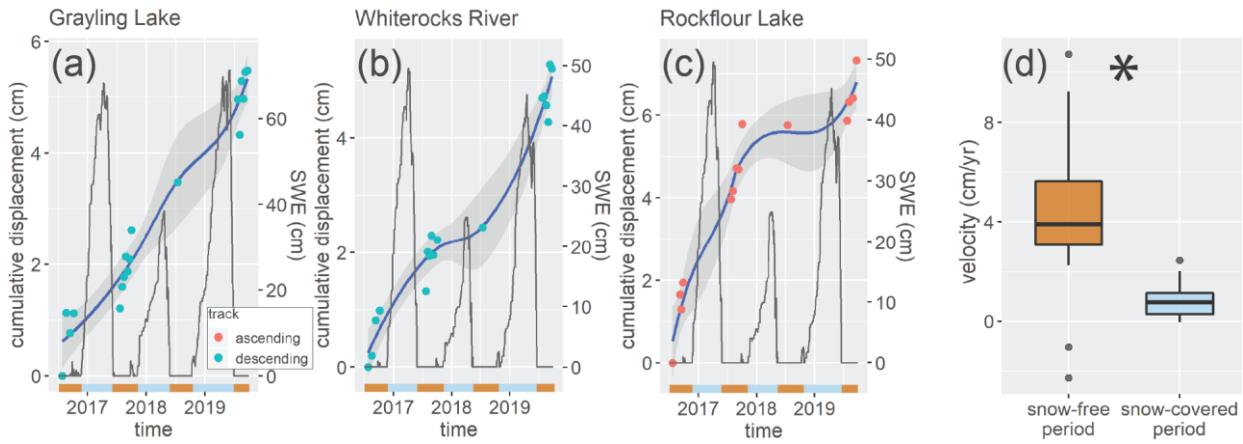
Figure 8. Displacement time series for three representative rock glaciers. (a, b, c) Time-dependent displacement of three rock glaciers from 2016-2019 and snow-water equivalent (SWE) from nearby weather stations. Blue and orange bars along the x-axes denotes snow-free (orange) and snow-covered (blue) periods. Ascending and descending LOS are scaled so they are both positive and increasing. Time series displacement values were calculated using an average of 9 pixels (8,100 m^2 total area) in the rock glacier. Interferograms with low overall coherence were manually removed from the time series. Gray shaded regions around trendlines are 95% confidence intervals. (d) LOS velocities of three rock glaciers during the snow-free period in late summer compared to the snow-covered period from October to July. $n = 30$, $p = 0.001$.
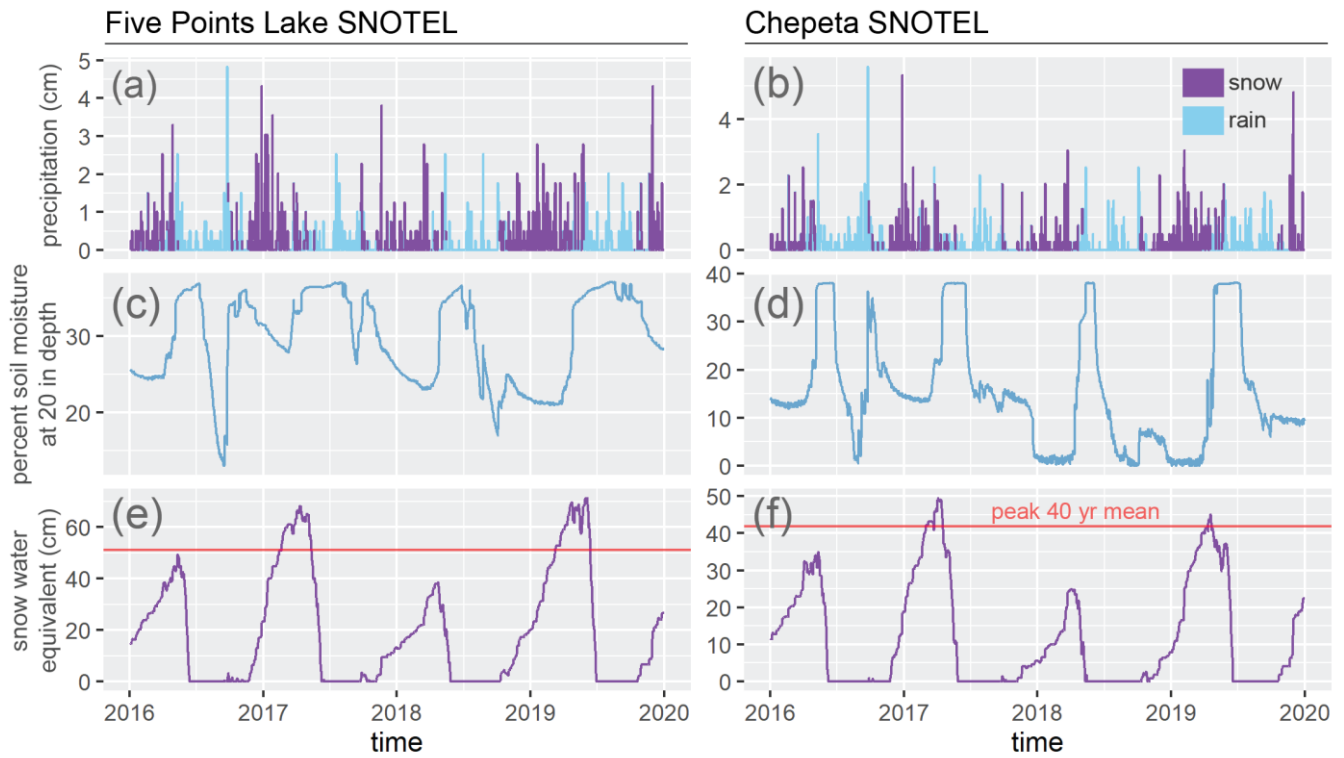
Figure 9. Precipitation, soil moisture, soil temperature, and snow water equivalent at the Five Points Lake and Chepeta SNOTEL stations from 2016−2019. (a, b) Precipitation events. Purple lines represent snow and blue lines represent rain. Precipitation type was inferred from average daily temperature at the SNOTEL station. (c, d) Percent soil moisture at 20 in depth. (e, f) Snow water equivalent (SWE). Red lines represent average peak SWE over the past 40 years.

865

870

875
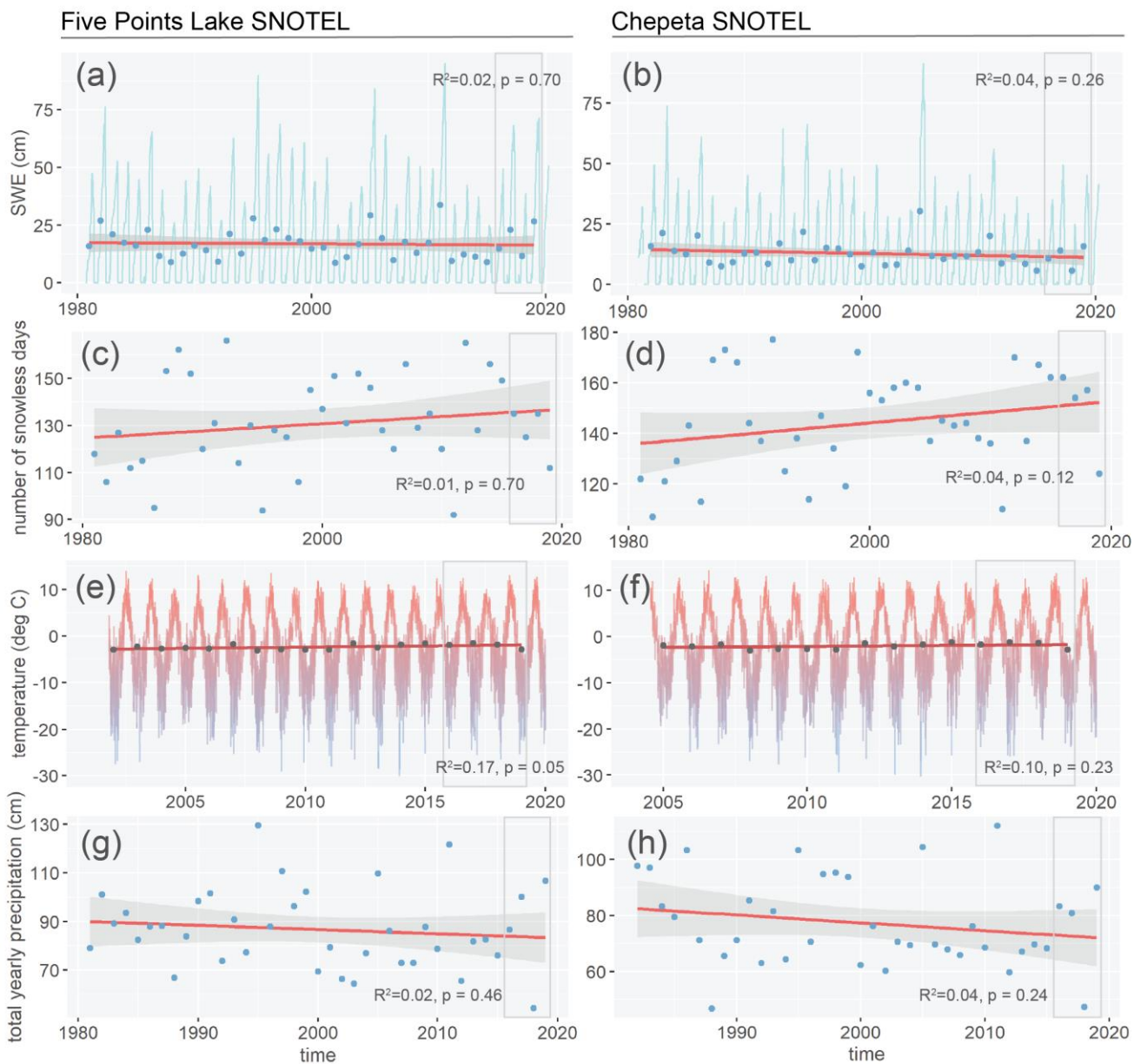
Figure 10. Climate over the past 40 years at the Five Points Lake SNOTEL (left) and Chepeta (right) SNOTEL stations. (a, b) Snow water equivalent (SWE). The light blue line is daily SWE. The dark blue points are mean annual SWE. (c, d) Number of days with no snow cover. Blue points represent number of days per year where SWE is 0. (e, f) Temperature over time. Blue to red regions represent daily temperature. Grey points are mean annual air temperature. (g, h). Mean annual precipitation over time. Blue points represent mean annual precipitation. For all, red lines are linear trendlines, and gray regions around lines are 95% confidence intervals. Gray boxes represent the study period.
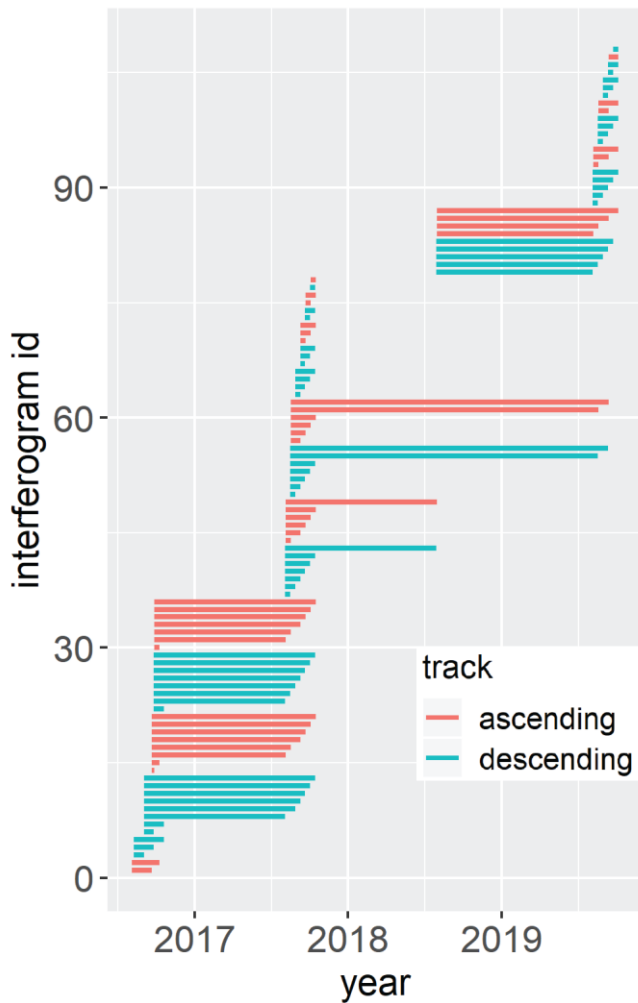
885

Figure A1. Temporal distribution of interferograms. Interferograms were generated using Sentinel 1 IW SLC scenes. Interferogram pairs were chosen based on snow-free periods. Red and blue lines represent ascending and descending interferograms, respectively.

890 **Table A1.** Track, date, and time span of all interferograms generated. Pairs that were averaged to create the ascending and descending one-year stacks used to estimate LOS velocities of rock glaciers are bolded.

number	track	primary acquisition date (yyymmdd)	secondary acquisition date (yyyymmdd)	timespan (days)
1	T122 ascending	20160804	20160921	48
2	T122 ascending	20160921	20160927	6
3	T122 ascending	20160804	20161009	66

4	T122 ascending	20160921	20161009	18
5	T122 ascending	20160927	20161009	12
6	T122 ascending	20160921	20170805	318
7	T122 ascending	20160927	20170805	312
8	T122 ascending	20160921	20170817	330
9	T122 ascending	20160927	20170817	324
10	T122 ascending	20170805	20170817	12
11	**T122 ascending**	**20160921**	**20170910**	**354**
12	T122 ascending	20160927	20170910	348
13	T122 ascending	20170805	20170910	36
14	T122 ascending	20170817	20170910	24
15	**T122 ascending**	**20160921**	**20170922**	**366**
16	**T122 ascending**	**20160927**	**20170922**	**360**
17	T122 ascending	20170805	20170922	48
18	T122 ascending	20170817	20170922	36
19	T122 ascending	20170910	20170922	12
20	T122 ascending	20160921	20171004	378
21	T122 ascending	20160927	20171004	372
22	T122 ascending	20170805	20171004	60
23	T122 ascending	20170817	20171004	48
24	T122 ascending	20170910	20171004	24
25	T122 ascending	20170922	20171004	12
26	T122 ascending	20160921	20171016	390
27	T122 ascending	20160927	20171016	384
28	T122 ascending	20170805	20171016	72
29	T122 ascending	20170817	20171016	60
30	T122 ascending	20170910	20171016	36
31	T122 ascending	20170922	20171016	24
32	T122 ascending	20171004	20171016	12
33	**T122 ascending**	**20170805**	**20180731**	**360**
34	**T122 ascending**	**20180731**	**20190807**	**372**
35	T122 ascending	20170817	20190819	732
36	T122 ascending	20180731	20190819	384
37	T122 ascending	20190807	20190819	12
38	T122 ascending	20170817	20190912	756
39	T122 ascending	20180731	20190912	408
40	T122 ascending	20190807	20190912	36
41	T122 ascending	20190819	20190912	24
42	T122 ascending	20180731	20191006	432
43	T122 ascending	20190807	20191006	60

44	T122 ascending	20190819	20191006	48
45	T122 ascending	20190912	20191006	24
46	T27 descending	20160809	20160902	24
47	T27 descending	20160809	20160926	48
48	T27 descending	20160902	20160926	24
49	T27 descending	20160809	20161020	72
50	T27 descending	20160902	20161020	48
51	T27 descending	20160926	20161020	24
52	T27 descending	20160902	20170804	336
53	T27 descending	20160926	20170804	312
54	T27 descending	20160926	20170816	324
55	T27 descending	20170804	20170816	12
56	**T27 descending**	**20160902**	**20170828**	**360**
57	T27 descending	20160926	20170828	336
58	T27 descending	20170804	20170828	24
59	T27 descending	20170816	20170828	12
60	**T27 descending**	**20160902**	**20170909**	**372**
61	T27 descending	20160926	20170909	348
62	T27 descending	20170804	20170909	36
63	T27 descending	20170816	20170909	24
64	T27 descending	20170828	20170909	12
65	T27 descending	20160902	20170921	384
66	**T27 descending**	**20160926**	**20170921**	**360**
67	T27 descending	20170804	20170921	48
68	T27 descending	20170816	20170921	36
69	T27 descending	20170828	20170921	24
70	T27 descending	20170909	20170921	12
71	T27 descending	20160902	20171003	396
72	T27 descending	20160926	20171003	372
73	T27 descending	20170804	20171003	60
74	T27 descending	20170816	20171003	48
75	T27 descending	20170828	20171003	36
76	T27 descending	20170909	20171003	24
77	T27 descending	20170921	20171003	12
78	T27 descending	20160902	20171015	408
79	T27 descending	20160926	20171015	384
80	T27 descending	20170804	20171015	72
81	T27 descending	20170816	20171015	60
82	T27 descending	20170828	20171015	48
83	T27 descending	20170909	20171015	36

84	T27 descending	20170921	20171015	24
85	T27 descending	20171003	20171015	12
86	**T27 descending**	**20170804**	**20180730**	**360**
87	**T27 descending**	**20180730**	**20190806**	**372**
88	T27 descending	20170816	20190818	732
89	T27 descending	20180730	20190818	384
90	T27 descending	20190806	20190818	12
91	T27 descending	20180730	20190830	396
92	T27 descending	20190806	20190830	24
93	T27 descending	20190818	20190830	12
94	T27 descending	20170816	20190911	756
95	T27 descending	20180730	20190911	408
96	T27 descending	20190806	20190911	36
97	T27 descending	20190818	20190911	24
98	T27 descending	20190830	20190911	12
99	T27 descending	20180730	20190923	420
100	T27 descending	20190806	20190923	48
101	T27 descending	20190818	20190923	36
102	T27 descending	20190830	20190923	24
103	T27 descending	20190911	20190923	12
104	T27 descending	20190806	20191005	60
105	T27 descending	20190818	20191005	48
106	T27 descending	20190830	20191005	36
107	T27 descending	20190911	20191005	24
108	T27 descending	20190923	20191005	12
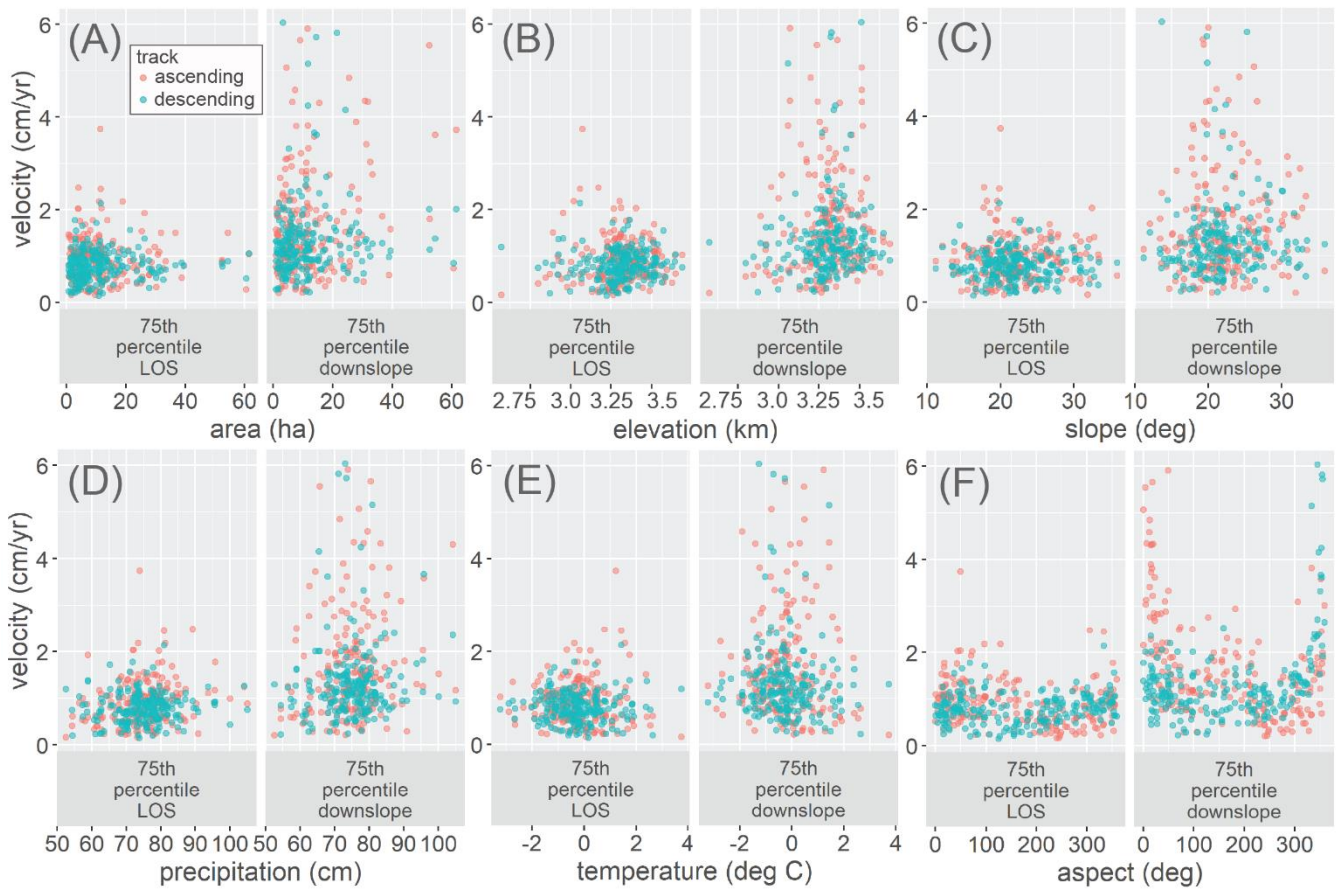
895

Figure A2. Rock glacier velocity plotted against physical variables and climate envelope. In all plots, velocity is the absolute value of 75th percentile LOS velocity on the right and 75th percentile downslope velocity on the right, compared to (a) rock glacier area, (b), rock glacier elevation, (c) rock glacier slope, (d) rock glacier mean annual precipitation, (e) rock glacier mean annual air temperature, and (f) rock glacier aspect. Two velocity values are presented for each rock glacier; One is derived

900 from the ascending one-year stack (red) and one from the descending one-year stack (blue). Temperature and precipitation data are from PRISM. n = 205.